MR/PET – Clinical Indications

Henryk Barthel
Department of Nuclear Medicine, University of Leipzig, Germany

Thomas Beyer
Medical University of Vienna, Center for Medical Physics and Biomedical Engineering, QIMP Team, Vienna, Austria

Onofrio A. Catalano
Massachusetts General Hospital, Harvard Medical School, Boston, MA, USA /
University of Naples, Parthenope, Naples, Italy

Zahi A. Fayad
Translational and Molecular Imaging Institute, Icahn School of Medicine at Mount Sinai, New York, NY, USA

Michael Kean
Murdoch Children's Research Institute, Parkville, VIC, Australia /
Royal Children's Hospital, Melbourne, VIC, Australia

Osama Sabri
Department of Nuclear Medicine, University of Leipzig, Germany

Michiro Sasaki
Sagara Perth Avenue Clinic, Kagoshima, Japan

Heinz-Peter Schlemmer
German Cancer Research Center, Heidelberg, Germany

Solveig Tiepolt
Department of Nuclear Medicine, University of Leipzig, Germany

Lale Umutlu
University Hospital Essen, University of Duisburg-Essen, Essen, Germany

siemens.com/magnetom-world

SIEMENS Healthineers

MR/PET Imaging Ready for Clinical Adoption

Thomas Beyer, Ph.D., MBA[1]; Antonis Kalemis, Ph.D. MBA[2]

[1] Medical University of Vienna, Center for Medical Physics and Biomedical Engineering, QIMP Team, Vienna, Austria
[2] Siemens Healthineers, Molecular Imaging, Erlangen, Germany

Hybrid imaging has been around for decades [1]. It represents an endeavor to better understand a clinical situation by combining information from complementary imaging modalities. The expectation is that each component will provide valuable insights with the integration of both representing more than the sum of the two modalities [2]. In the early years of complementary imaging, in the late 1960s, it was about drawing anatomical contours on scintigraphy plots. In the 1970s, the first combined transmission and emission scans were performed. A decade later, computers were employed to align complementary image sets in order to better describe the disease-related foci. Following these very diverse approaches to combine two or more sets of imaging information as part of patient management, today, hybrid imaging denotes the hardware combination of two complementary imaging modalities.

Hybrid imaging had a headstart in the 1990s with multiple groups approaching different combinations of imaging technologies at about the same time. Bruce Hasegawa and colleagues proposed a combined SPECT/CT system in 1992 [3], although the first patent for a combined SPECT and CT was filed by Ukrainian scientist Mirshanov in 1986 [4]. In 1993, Bruce Hammer filed a patent application for the first MR/PET system [5]. And in 1998, images from the first whole-body PET/CT system were presented by David Townsend and team during the Annual Meetings of the Society of Nuclear Medicine Meeting and the Radiological Society of North America [6]. However, the first PET/CT system – originally employed for neuro-oncology imaging – was built by a team of clinical scientists at Gunma University in Japan in 1982.

MR/PET is really the most up-to-date implementation of hybrid imaging in clinics today. It was only after major technical challenges were overcome that the combination of MRI and PET became fit for routine adoption [7, 8]. Hybrid imaging physically combines two imaging systems thus requiring the close spatial proximity of the two modalities. PET is based on the use of scintillation crystals coupled to photomultipliers that help decode the origin of the incoming annihilation photons and thus the activity distribution in the patient. The detection system employs Anger logic, a simple weighting of secondary signals named after a pioneer of nuclear medicine imaging, Hal A. Anger. Photomultipliers (PMTs) are multi-stage signal amplifiers that are based on electrical fields in a sequential arrangement of photocathodes in a vacuum tube. When placed in the vicinity of a magnetic field, this amplification process falters and no meaningful signal or position map can be derived. Placing a standard PET and MRI, which operates at a 1.5T magnetic field strength or higher, close together is therefore not feasible.

This methodological and technical challenge was addressed by the early developers of MR/PET in two ways. One solution was to move the PMTs outside the magnetic field and to separate them from the scintillation crystals by means of a lightguide. This was adopted for pilot pre-clinical systems. The second proposed solution was to place the PET and MR a certain distance from each other, which was the solution used in commercial whole-body MR/PET systems [9]. Neither approach, however, was capable of releasing the intrinsic potential of combined MR/PET, which is to acquire the emission and MR data simultaneously.

Such acquisition required the full integration of the MR and PET components, which was only made possible with the development of solid-state detectors that were inert to magnetic fields, unlike the previous PMTs [10]. The first fully-integrated MR/PET system was proposed by Siemens in 2006 and comprised an APD-based PET detector ring that could be fitted into a MAGNETOM Trio 3T MRI to provide combined MR/PET imaging of the human brain [11]. The first pilot systems were installed between 2006 and 2008 and greatly advanced the development of combined MR/PET. Testing such combination imaging systems in clinical routine and in the review of clinical proof points did yield major challenges. Moreover, the validation of attenuation and scatter correction of the emission data in the absence of a standard transmission scan was an early key obstacle and, indeed, a bottleneck in the clinical testing of MR/PET. Numerous studies have been published over the years that commonly derive a transmission-like attenuation map from complementary MR images acquired as part of the combined examination [12]. This derivation can be tailored to a given patient by using dedicated MR sequences, such as the in- and opposed-phase Dixon sequence proposed by Martinez-Möller [13], or the ultrashort time echo (UTE) imaging sequence proposed by Catana et al. [14]. Recently, machine-learning approaches have also been employed to derive MR-based attenuation maps (MR-AC) [15]. In general, these approaches are effective and residual variations in attenuation coefficients with respect to the gold or silver standard of PET-based and CT-based transmission imaging, respectively, are much lower than the general variation in PET quantification from non-standardized imaging procedures. As stated by an expert panel during a recent International PET/MR Workshop in Tübingen: "The case of MR-based attenuation correction is closed." [16]

By accepting this conclusion, the field has become open to pushing the boundaries of combined MRI/PET in clinical research in particular. Today, a decade into commercial MR/PET, there are over 150 installations worldwide (Fig. 1) engaging in clinical imaging and research activities.

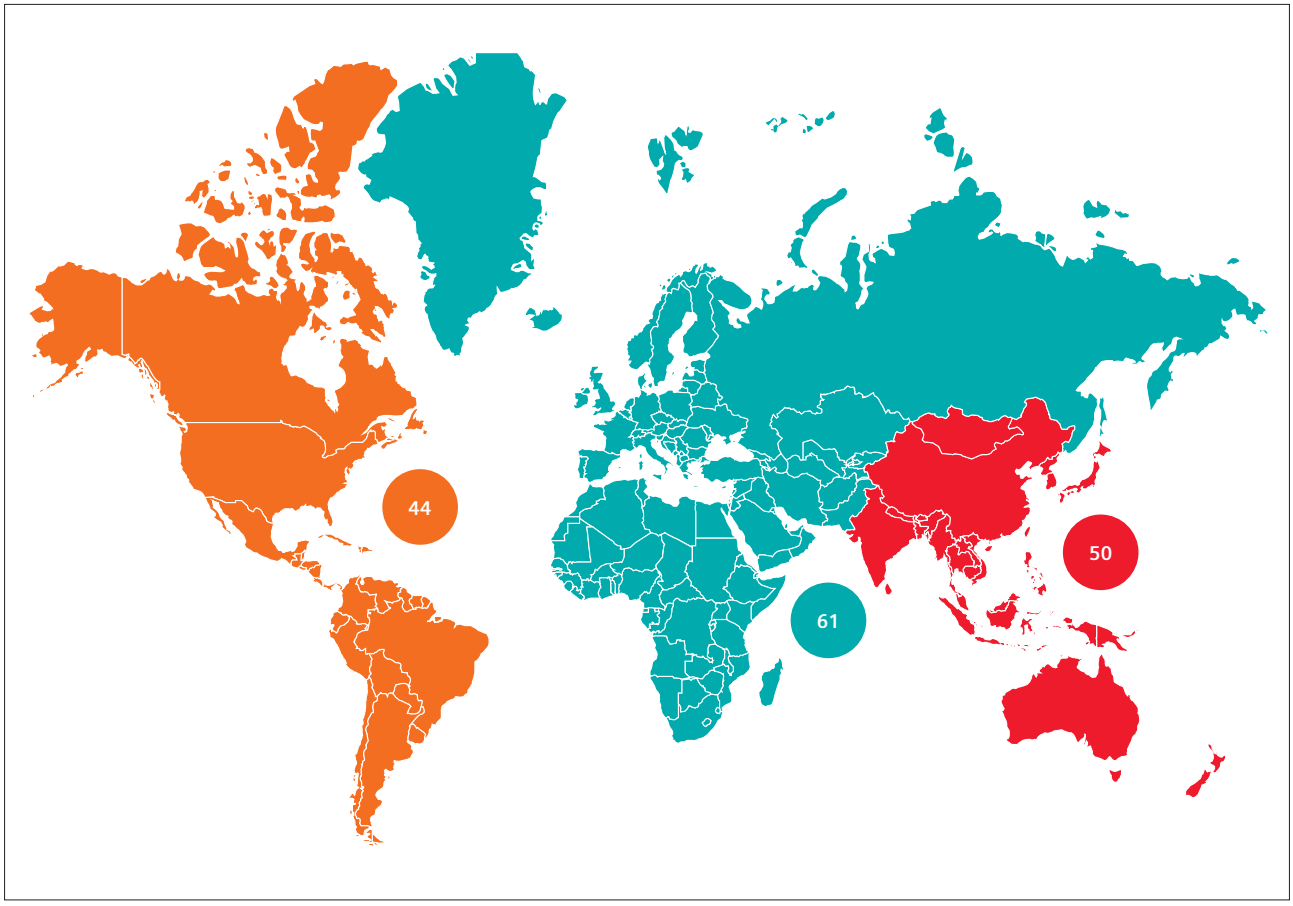

1 Nine years after the first clinical PET/MR systems were introduced, installations can be found in every continent. The map above illustrates the spread of such systems by continent/market.

In the early years of MR/PET, the aim of the clinical community was to build on the success of PET/CT and provide similar types of diagnostics while lowering the exposure of patients to ionizing radiation by substituting CT imaging with PET-based hybrid imaging. This perspective was shared by many in the field given the possible reduction of radiation exposure in patients who were not diagnosed with terminal illnesses but who had a very good long-life prognosis, such as children or patients with mental impairments. Overall, the effective dose for patients undergoing a combined, whole-body MR/PET imaging examination using ^{18}F-FDG versus a similar examination with PET/CT and CT contrast agent (to account for the high soft tissue contrast in MRI) can be on the order of 60–70% down to about 7 mSv, or less.

Now a number of years into the clinical use of MR/PET, two meta-analyses have demonstrated a comparable diagnostic accuracy of MR/PET and PET/CT, at least for oncologic indications [17]. This is an important finding considering what an arduous undertaking it has been to advance MR/PET from a pilot imaging system for humans in 2006 to a clinical, whole-body modality in 2011, based on a detector technology that has only recently become more widely used. MR/PET can thus be regarded a technical revolution supporting a diagnostic evolution.

The present compendium of clinical perspectives is an effective illustration of this development. This booklet brings together leading experts in the field who share with you, the reader, their experience and perspectives on the state-of-the-art of fully-integrated MR/PET in a broad spectrum of clinical indications within oncology, neurology, and cardiology. In addition to providing routine complementary molecular information from the PET scan and anatomical and tissue-specific information from the MRI scan, MR/PET provides patients with logistical benefits. These are perhaps most important for patients who may require sedation such as those with mental disorders, the very ill, or the very young[1]. Moreover, fully-integrated MR/PET has the potential to bring additional synergy effects from the two modalities, such as MR-based motion compensation of the PET or MR-based partial volume correction, each of which is beneficial for imaging organs that are subject to significant motion (e.g., lungs, liver, lower abdomen, and heart) or small-size regions (lesions and plaques). The combination of both techniques is an important step in the recent pursuit of non-invasive approaches to multiparametric imaging that include the use of an image-derived input function for quantitative PET [18]. The two methods taken together represent an exciting development in imaging technology, which broadens the application of non-invasive diagnostic means to the benefit of patients worldwide. This booklet is testimony to the potential of this development.

Contact

Thomas Beyer, PhD, MBA
Professor of Physics in Medical Imaging
Medical University of Vienna
Center for Medical Physics and
Biomedical Engineering
QIMP Team
General Hospital Vienna, 4L
Waehringer Guertel 18-20
A-1090 Vienna
Austria
Tel.: +43 1 40400 39890
thomas.beyer@meduniwien.ac.at

References

1 Townsend D. Multimodality imaging of structure and function. Phys Med Biol 2008; 53(4): R1-R39.
2 Beyer T, et al. 1 + 1 = 3. Nuklearmedizin 2005; 44(5a): S1.
3 Hasegawa B, et al. A Prototype High-Purity Germanium Detector System with Fast Photon-Counting Electronics for Medical Imaging. Medical Physics 1991; 18: 900-909.
4 http://www.iaea.org/inis/collection/NCLCollectionStore/_Public/21/011/21011271.pdf
5 Hammer B. NMR-PET Scanner Apparatus. U.S. Patent July 3, 1990. USA.
6 Townsend D, et al. The SMART Scanner: A combined PET/CT tomograph for clinical oncology. Radiology 1998; 209 (P): 169-170.
7 Wehrl H, et al. Pre-clinical PET/MR: technological advances and new perspectives in biomedical research. Eur J Nucl Med Mol Imag 2009; 36(suppl. 1): S56-S68.
8 https://www.ncbi.nlm.nih.gov/pubmed/28431784
9 Kalemis A, et al. Sequential whole-body PET/MR scanner – concept, clinical use and optimisations after two years in the clinic. The manufacturer's perspective. MAGMA 2012; 25(1): 5-23.
10 https://www.ncbi.nlm.nih.gov/pubmed/9517036
11 Schlemmer H, et al. Simultaneous MR/PET imaging of the human brain: feasibility study. Radiology 2008; 248(3): 1028-1035.
12 Wagenknecht G, et al. MRI for attenuation correction in PET: methods and challenges. MAGMA 2013; 26(1): 99-113.
13 Martinez-Möller A, et al. Tissue classification as a potential approach for attenuation correction in whole-body PET/MRI: evaluation with PET/CT data. J Nucl Med 2009; 50(4): 520-526.
14 Catana C, et al. Toward implementing an MRI-Based PET attenuation-correction method for Neurologic studies on the MR-PET brain prototype. J Nucl Med 2010; 51:1431-1438.
15 Paulus DH, et al. Whole-Body PET/MR Imaging: Quantitative Evaluation of a Novel Model-Based MR Attenuation Correction Method Including Bone. J Nucl Med. 2015 Jul;56(7):1061-6. doi: 10.2967/jnumed.115.156000. Epub 2015 May 29.
16 Bailey D, et al. Combined PET/MRI: Global Warming-Summary Report of the 6th International Workshop on PET/MRI, March 27-29, 2017, Tübingen, Germany. Mol Imaging Biol 2017 Oct 02; 20(1).
17 Spick C, et al. 18F-FDG PET/CT and PET/MRI Perform Equally Well in Cancer: Evidence from Studies on More Than 2,300 Patients. J Nucl Med 2016; 57(3): 420-430.
18 Sundar L, et al. Towards quantitative [18F]FDG-PET/MRI of the brain: Automated MR-driven calcuation of an image-derived input function for the non-invasive determination of cerebral glucose metabolic rates. JCBFM 2018. DOI: 10.1177/0271678X18776820.

The Role of MR/PET for Breast Cancer Treatment Strategies

Michiro Sasaki[1]; Mitsuhiro Tozaki[2]; Yoshiaki Sagara[2]

[1] Department of Radiology, Sagara Perth Avenue Clinic, Kagoshima, Japan
[2] Department of Radiology, Sagara Hospital Affiliated Breast Center, Kagoshima, Japan

Introduction

For breast cancer examinations, MR/PET is a very useful modality as it allows morphological (MRI) and biological (PET) evaluation of primary tumors as well as assessment of distant metastases in the whole body.

Hakuaikai Sagara Hospital, which specializes in women's health and well-being, installed MR/PET in its Sagara Perth Avenue Clinic in September 2016 and it became operational one month later.

Indications

Medical examinations are conducted mainly for cancer screening, preoperative examination, and post-operative follow-up of breast cancer. In addition, preoperative staging and postoperative follow-up assessment of any metastatic disease for thyroid, prostate, and gyneco-logical malignancies are also conducted frequently.

The total number of examinations from October 31, 2016 to October 31, 2017 was 1,099 (including MRI only). These included 253 cancer screenings, 555 preoperative examinations of breast cancer, and 187 examinations for the purpose of searching metastatic recurrence after breast cancer surgery.

Imaging protocol

In cancer screening, preoperative examination of breast cancer and postoperative follow-up, whole-body scans are first acquired in the supine position. MR imaging is based on a transverse image of T1-weighted (Dixon VIBE), T2-weighted half-Fourier single-shot turbo spin-echo (HASTE), and diffusion-weighted imaging (DWI; b (in s/mm^2) = 0, b = 800). Dixon VIBE and HASTE imaging is conducted under breath-holding guidance for respiratory motion management in the abdomen and chest. Axial T1-weighted VIBE and HASTE sequences and axial DWI (b = 0, b = 800) were obtained during simultaneous PET acquisition. Four to five PET bed positions from head to thighs were usually required, depending on the patient's height. The emission time per bed was 4 minutes. In the preoperative examination of breast cancer, after whole-body PET/MR is completed, dedicated breast MR/PET is performed with the patients in the prone position. The breast MR/PET comprises a breast PET scan of 1 bed position and a simultaneous breast MRI using a standard 4-channel Breast Coil. The emission time of the PET scan is 15 minutes. The breast MRI examination consisted of a localizer sequence, coronal T1-weighted turbo spin-echo (TSE), and sagittal T2-weighted fat-suppressed TSE sequence, coronal a single-shot echo planar DWI (b = 0, b = 1000), and 3D dynamic contrast-enhanced (DCE) sequence. DCE-MRI was performed with coronal T1-weighted fat-suppressed 3D VIBE, with one pre-contrast and three post-contrast dynamic series performed within 5 minutes depending on the breast thickness after bolus injection. Next, 1 mL/s of gadobutorol (0.1 mmol/kg of body weight, Gadovist; Bayer Schering Pharma, Berlin, Germany) is injected, followed by a 20 mL saline flush (Table 1).

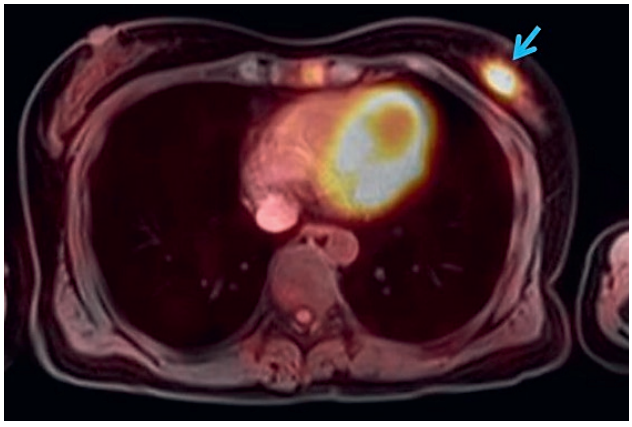

1 Case 1

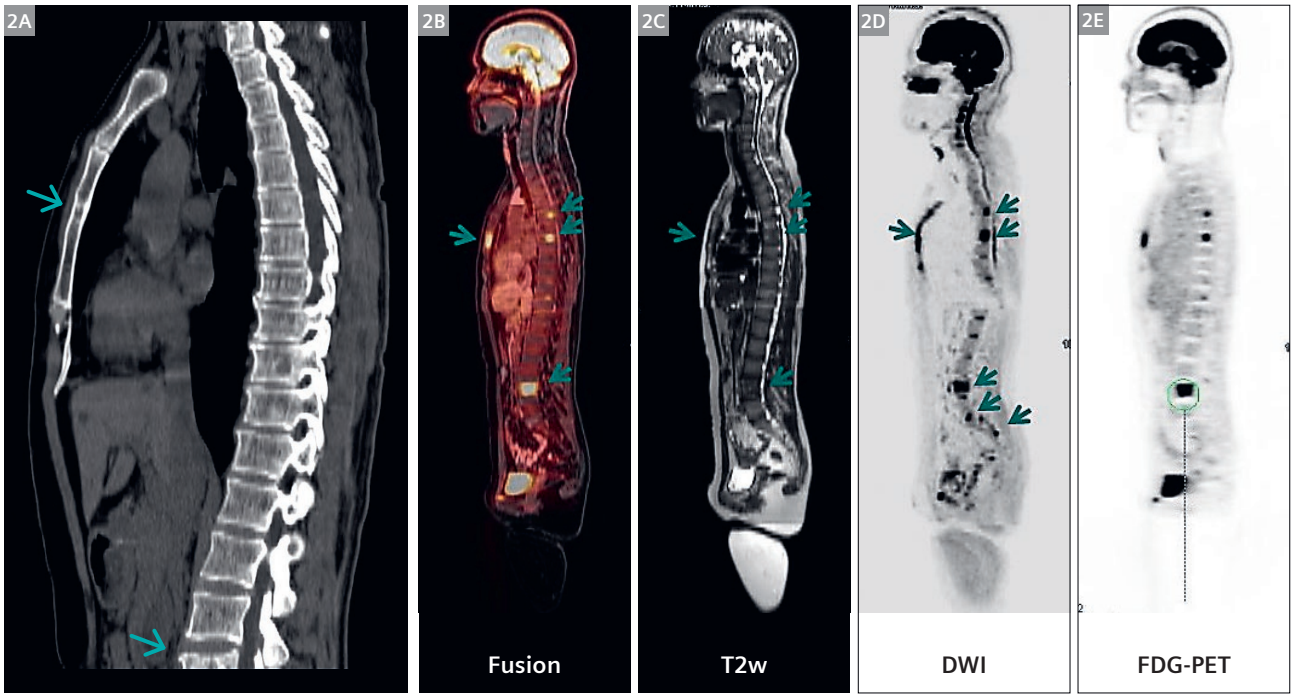

2 Case 1

Benefits of MR/PET

As a preoperative examination of breast cancer, combining PET and MRI in one system allows the clinician to diagnose local spread (breast) and the spread in the whole body (search for metastases) at the same time. The high FDG accumulation in sites suspicious for metastases can guide through investigation by MRI that can confirm or reject suspicion and in this manner boost the overall accuracy of the investigation. Below are some indicative cases for which MR/PET imaging seems to be useful.

Case 1

A woman in her 40s referred for examinations by her physician due to an identified suspicious breast mass. Mammography and ultrasound diagnosed cancer in the left breast (cT2N0Mx cStage IIA), and MR/PET imaging was performed as a preoperative examination. A primary tumor showing an abnormal accumulation of FDG in the left breast is depicted in the fusion image (Fig. 1). In sagittal view of the whole-body image, multiple bone metastases are also clearly depicted. Final imaging diagnosis was upstaging with left breast cancer; cT2N0M1, cStage IV. A CT scan also hinted bone metastases (Fig. 2A), but these can be evaluated in detail on PET/MRI (Figs. 2B–2E).

In our data, bone metastases were found by MR/PET in three cases (1.2%, Luminal A in 2, HER 2 type in 1) of breast cancer patients (cStage I to II) who underwent a pre-operative examination, so they were upstaged to cStage IV. These results are in accordance with one present study where 11 out of 111 patients (9.9%) with primary breast cancer under the age of 40 in pre-examination stages I to II were found to have distant metastases using PET/CT and upstaged to Stage IV [1]. Another study reports that 8 cases of distant metastases were found by PET/CT for preoperative examination in 115 early-stage (Stage I to II) breast cancer patients [2].

Cases 2 and 3

Two female patients with breast cancer are presented below (Figs. 3A and 3B, respectively). The first in her 70s (IDC [scirrhous carcinoma], histological tumor spread 21 mm, infiltration diameter 21 mm, ER: positive PgR: positive) and the second in her 50s (IDC [scirrhous carcinoma], histological tumor spread and tumor invasion diameter 24 mm, ER: positive, PgR: positive). Although tissue type (Figs. 5 and 6), tumor size and hormonal expression status were similar, the SUV_{max} values on PET/MRI were different between the two cases, 1.79 and 6.46, respectively. Further investigations showed the presence of HER2 receptors in the second case, which may explain the accumulation differences of FDG (Fig. 4). In these two cases, in addition to qualitative diagnosis of tumor and diagnosis of tumor spread by dynamic MRI, quantitative PET/MRI allowed the possibility to differentiate the tumor's proliferation capacity (aggressiveness). By acquiring PET data simultaneously to MRI makes it possible to obtain such prognostic-relation information which is very important for breast cancer treatment strategies.

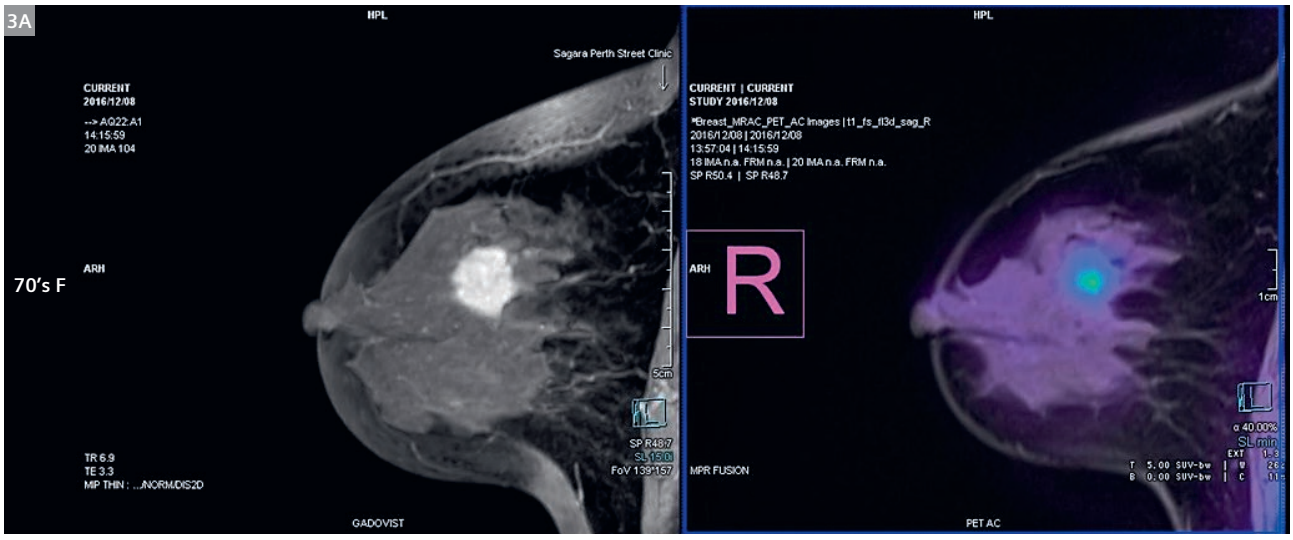

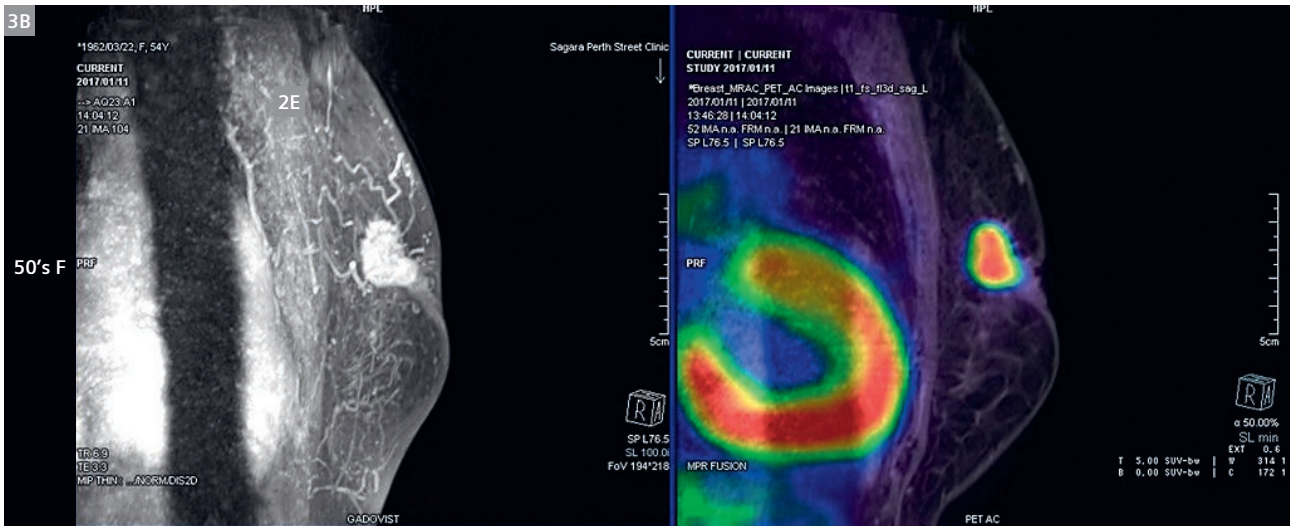

	70's F	50's F
Tumor size	21 x 12 x 10 mm	24 x 18 x 16 mm
ER	+	+
PgR	+	+
HER2	–	+
Nuclear grade	2	2
Ki67	–	+
ly	–	+

Table 1: Association between tumor status and tumor SUV_{max}.

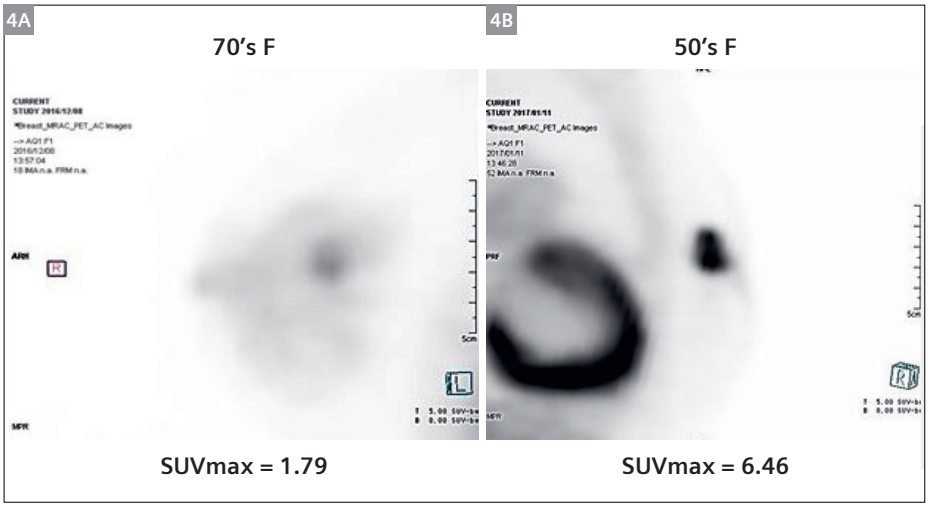

3 + 4 Case 2 and 3

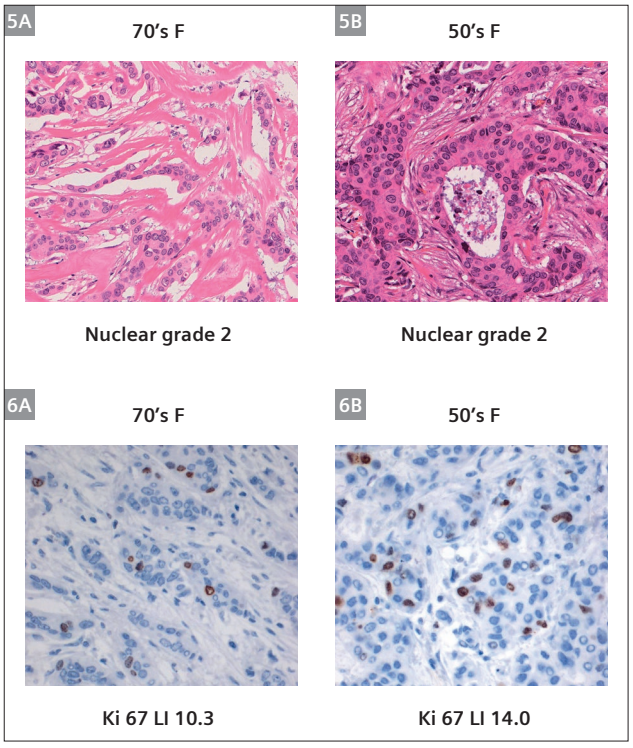

5 + 6 Case 2 and 3

Conclusion

We examined and presented on the relationship between SUV and ADC value and prognostic related pathological factors obtained by simultaneous imaging in 94 cases 100 lesions in which MR/PET imaging was performed as a preoperative examination. Among them, SUV_{max} showed association with tumor size, HER2 receptor, nuclear grade, Ki-67 in univariate analysis. However, ADC_{mean} correlated only with Nuclear grade. Furthermore, there is no correlation between ADC-breast and SUV-breast, and both may reflect different biology [3]. Combining both SUV and ADC data can be a new indicator of breast cancer biology assessment. Therefore, MR/PET, being able to obtain two data at the same time, is a very useful examination. Accordingly, we are currently conducting verifications by increasing the number of cases.

The accuracy of the whole-body DWI method used for the above studies was a limitation. However, further improvements in the precision of DWI methods is anticipated, and novel methods, such as RESOLVE are expected to improve significantly the accuracy of this method. For this reason our department works together with Siemens Healthineers for improving the detection sensitivity of breast cancer.

References

1 Christopher C, et al.: Retrospective Analysis of ^{18}F-FDG PET/CT for Staging Asymptomatic Breast Cancer Patients Younger Than 40 Years. J Nucl Med 55(10): 1578-1583, 2014.
2 Garami, et al.: The value of ^{18}F-FDG PET/CT in early-stage breast cancer compared to traditional diagnostic modalities with an emphasis on changes in disease stage designation and treatment plan. EJSO 38: 31-37, 2012.
3 Sasaki M, Tozaki M et al.: Simultaneous whole-body and breast ^{18}F-FDG PET/MRI examinations in patients with breast cancer: a comparison of apparent diffusion coefficients and maximum standardized uptake values. Jpn J Radiol. 2018;36(2): 122-133.

Further reading

For more information on breast imaging with MR/PET the interested readers can look at the following publications:

1 Grueneisen J, Sawicki LM, Wetter A, Kirchner J, Kinner S, Aktas B, et al.: Evaluation of PET and MR datasets in integrated ^{18}F-FDG PET/MRI: A comparison of different MR sequences for whole-body restaging of breast cancer patients. Eur J Radiol. 2017; 89: 14-9.
2 Taneja S, Jena A, Goel R, Sarin R, Kaul S.: Simultaneous whole-body F-FDG PET-MRI in primary staging of breast cancer: a pilot study. Eur J Radiol. 2014; 83: 2231-9.
3 Botsikas D, Kalovidouri A, Becker M, Copercini M, Djema DA, Bodmer A, et al.: Clinical utility of ^{18}F-FDG-PET/MR for preoperative breast cancer staging. Eur Radiol. 2016; 26: 2297-307.
4 Kong EJ, Chun KA, Bom HS, Lee J, Lee SJ, Cho IH.: Initial experience of integrated PET/MR mammography in patients with invasive ductal carcinoma. Hell J Nucl Med. 2014; 17: 171-6.
5 Catalano OA, Daye D, Signore A, Iannace C, Vangel M, Luongo A, et al.: Staging performance of Whole-body DWI, PET/CT and PET/MRI in invasive ductal carcinoma of the breast. International J Oncology. 2017, 51: 281-8.
6 Catalano OA, Rosen BR, Sahani DV, Hahn PF, Guimaraes AR, Vangel MG, et al.: Clinical impact of PET/MR imaging in patients with cancer undergoing same-day PET/CT: Initial experience in 134 patients – a hypothesis-generating exploratory study. Radiology. 2013; 269: 857-69.
7 Zhang H, Xue H, Alto S, Hui L, Kannengiesser S, Berthold K, et al.: Integrated shimming improves lesion detection in whole-body diffusion-weighted examinations of patients with plasma disorder at 3T. Invest Radiol. 2016;51(5):297–305.
8 Wang J, Ting-Fang Shih T, Yen RF et al.: Multiparametric Evaluation of Treatment Response to Neoadjuvant Chemotherapy in Breast Cancer Using Integrated PET/MR. Clin Nucl Med 2017;00(00):1-8.

Contact

Michiro Sasaki
Department of Radiology
Sagara Perth Avenue Clinic
26-13 Shin-Yashikicho, Kagoshima City
Kagoshima 892-0838
Japan


Michiro Sasaki


Yoshiaki Sagara


Mitsuhiro Tozaki

Application of MR/PET in Prostate Cancer

Heinz-Peter Schlemmer, M.D., Ph.D.

Department of Radiology, German Cancer Research Center, Heidelberg, Germany

The most frequently occurring cancer in industrialized countries throughout the world is characterized by significant variations in multifocality and biological aggressiveness. Excellent long-term survival is achieved by radical prostatectomy or radiotherapy in case of localized disease [1]. But conventional diagnostic procedures using PSA-serum testing, digital rectal examination and systematic transrectal biopsy are known to be insufficient. Overdiagnosis of biologically insignificant disease is feared, because possible treatment-related side effects of impotence and incontinence have detrimental impact on the quality of life. However, undertreatment is also of concern, due to misdiagnosis including missed cancers, high-grade cancers being incorrectly classified as low, or the high risk of a missed cancer spreading. Improved diagnostics are urgently needed for personalized optimized therapies, in particular as less invasive treatment alternatives are currently emerging in order to minimize treatment side effects including e.g. laser, cryo, HIFU or IRE focal ablation therapies. Any achievements will have high medical and socioeconomic impact.

Individually-optimized treatment is based on the precision of cancer diagnosis concerning early detection, grading, and staging, for which high-quality imaging is essentially required for:

1. detection and localization of suspicious lesions within the prostate with high sensitivity and high negative predictive value;
2. precise and reliable tissue sampling from those lesions for accurate cancer detection and grading of individual biologic aggressiveness;
3. local T staging to assess tumor location(s), size(s), and possible extracapsular extension beyond the capsule and/or into the seminal vesicles, urethra, and/or urinary bladder;
4. distant N/M staging to identify distant cancer spreading to lymph nodes, bones or other organs; and
5. restaging in case of biochemical relapse after treatment in order to detect at an early stage and localize the recurrent cancer sites.

Over the last couple of years an increasing number of clinical studies have demonstrated that multiparametric MR imaging (mpMRI) is advantageous for initial diagnosis and local staging of prostate cancer. Combined risk models including clinical and mpMRI parameters offer significant improvement for prediction of clinically relevant prostate cancer and thereby to refine the indication for biopsy and to avoid unnecessary biopsies [2]. Transrectal or transperineal TRUS/MR image fusion biopsy methods including targeted +/- random biopsies of MR suspicious lesion have been proven to be beneficial for precise and reliable pathologic diagnosis [3, 4]. Meanwhile, several national guidelines have recommended prostate mpMRI in case of:

1. negative initial biopsy, but persistent clinical suspicion of prostate cancer;
2. active surveillance; and
3. pre-biopsy in selected cases.

Dissemination of high-quality mpMRI was initially hindered by a lack of standardized image acquisition, interpretation, and documentation, but the PI-RADS recommendations of the ESUR and ACR have brought about a considerable progress [5].

mpMRI is furthermore considered as the method of choice for local staging of prostate cancer. Macroscopic extracapsular cancer extension (ECE) can be detected with high specificity of ca. 95%. The contrasting low sensitivity of ca. 50% is due to the fact that microscopic cancer extension either in the capsule or the seminal vesicles can in principle not be visualized given the limited spatial resolution of MR [6]. The use of additional indicators including tumor size, capsule contact length, and dynamic contrast enhancement (DCE) characteristics can improve the prediction of ECE. But early detection of distant cancer spreading particularly into lymph nodes is in fact impossible using mpMRI. The method is furthermore insufficient for early detection and localization of recurrence in case of PSA relapse after curative intended therapy.

Cancer spreading and local recurrence are detected with highest sensitivity by PET. The "working horse" in clinical routine is whole-body PET/CT, which is robust, fast, relatively widely available, and cost-effective [7]. It is important to note, however, that the accuracy of PET/CT strongly depends on the applied radiotracer. In clinical routine, various radiotracers are currently in use, most commonly C-11 or F-18 choline and Ga-68 or F-18 PSMA. Recent multicentre studies have proven that PSMA PET/CT with Ga-68 PSMA-11 change the clinical management of prostate cancer patients in up to 50% of the cases [8, 9]. PSMA PET/CT has meanwhile emerged as standard for restaging in case of biochemical recurrence. But because CT is insufficient to visualize primary, recurrent and metastatic cancer due to its intrinsic low soft tissue contrast, PSMA negative cancer may be missed. The CT part of the PET/CT examination is basically used only for anatomical referencing (besides attenuation correction).

MR imaging including pelvic mpMRI plus whole-body MRI/DWI provides superior soft tissue. Accordingly, PSMA PET/MR creates opportunities by combining highest sensitivity of molecular imaging by PSMA-PET with best anatomical referencing and functional tissue assessment by MR. Synergistic information has been demonstrated recently for primary and recurrent prostate cancer [10, 11].

MpMRI has proven valuable for cancer detection and local T-staging. MR/TRUS fusion biopsy or MR-guided biopsy are the most accurate and widely accepted approaches for establishing the initial pathologic diagnosis. But possible distant tumor spreading cannot be detected or ruled out by MR alone. PSMA PET/MR offers the opportunity to complement mpMRI. Up to now, most PSMA PET/MR studies have focused on the detection of local recurrence and metastatic disease and PET/MR has proved to be diagnostically equal or even superior to PET/CT [10]. Indications could therefore include restaging in case of biochemical recurrence, assessment of high-risk patients

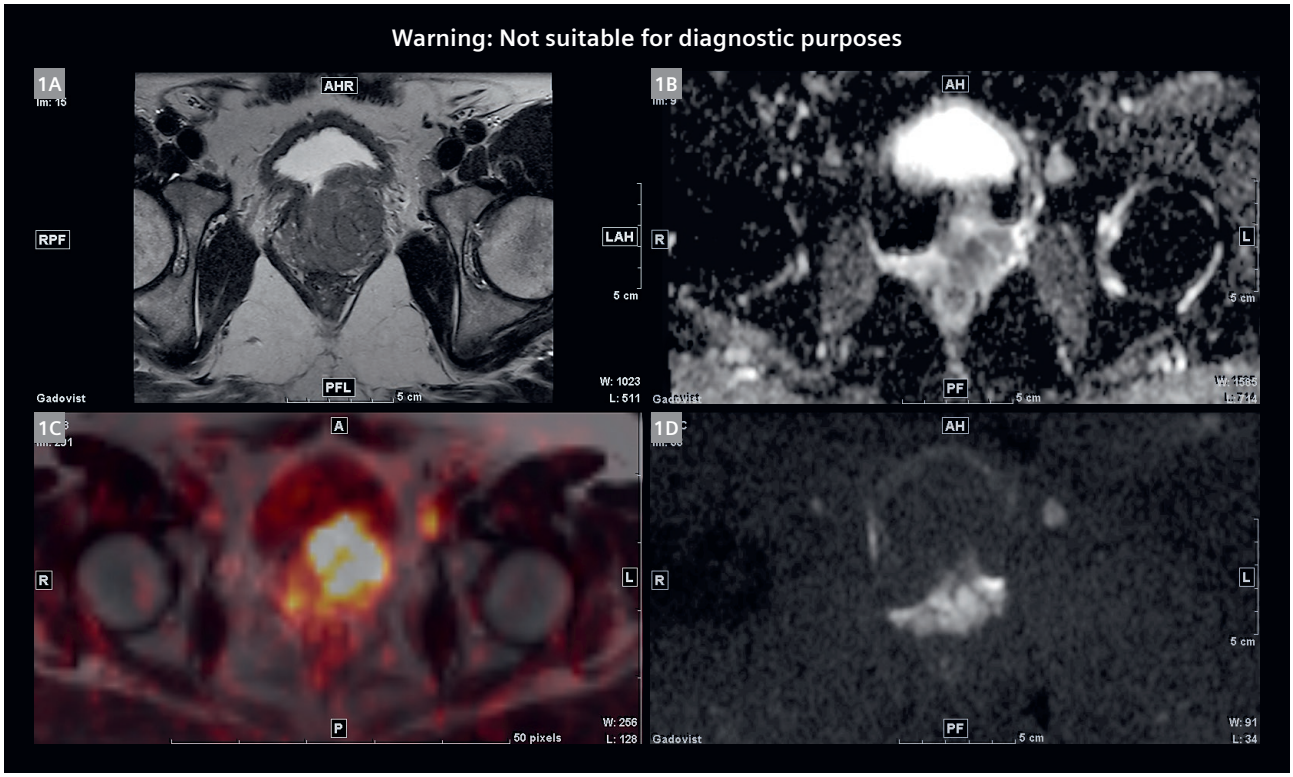

1 ^{18}F-PSMA PET/MR of a 54 y/o patient with PSA of 63.8 ng/ml. Advanced prostate cancer involving almost the entire prostate is visualized with characteristic MR appearance including diffusion restriction. PSMA-PET demonstrates typical tracer uptake of the cancer and indicates in addition two inguinal lymph node metastases on the right (11 mm) and the left (7 mm).

to detect/rule out metastatic disease (i.e. with proven Gleason grade ≥ 4+3 and/or extended prostate cancer), and maybe in the future also of patients with only the clinical suspicion of being at high risk (Fig. 1). A comprehensive PSMA-PET/MR examination protocol for clinical routine is feasible and can easily be implemented [12, 13]. Indications for PSMA-PET/MR include currently:

1. staging of high-risk patients;
2. detection of recurrence in case of PSA relapse; and
3. planning and monitoring of PSMA radionuclide therapy.

The diagnostic advantage of simultaneous PET/MR over sequentially performed PET/CT plus MR together with subsequent software image fusion has still to be evaluated, however [14].

References / Further reading

1 Hamdy FC, Donovan JL, Lane JA, Mason M, Metcalfe C, Holding P, Davis M, Peters TJ, Turner EL, Martin RM, Oxley J, Robinson M, Staffurth J, Walsh E, Bollina P, Catto J, Doble A, Doherty A, Gillatt D, Kockelbergh R, Kynaston H, Paul A, Powell P, Prescott S, Rosario DJ, Rowe E, Neal DE; ProtecT Study Group. 10-Year Outcomes after Monitoring, Surgery, or Radiotherapy for Localized Prostate Cancer. N Engl J Med. 2016 Oct 13;375(15):1415-1424.

2 Radtke JP, Wiesenfarth M, Kesch C, Freitag MT, Alt CD, Celik K, Distler F, Roth W, Wieczorek K, Stock C, Duensing S, Roethke MC, Teber D, Schlemmer HP, Hohenfellner M, Bonekamp D, Hadaschik BA. Combined Clinical Parameters and Multiparametric Magnetic Resonance Imaging for Advanced Risk Modeling of Prostate Cancer-Patient-tailored Risk Stratification Can Reduce Unnecessary Biopsies. Eur Urol. 2017 Dec;72(6):888-896.

3 Ahmed HU, El-Shater Bosaily A, Brown LC, Gabe R, Kaplan R, Parmar MK, Collaco-Moraes Y, Ward K, Hindley RG, Freeman A, Kirkham AP, Oldroyd R, Parker C, Emberton M; PROMIS study group. Diagnostic accuracy of multi-parametric MRI and TRUS biopsy in prostate cancer (PROMIS): a paired validating confirmatory study. Lancet. 2017 Feb 25;389(10071):815-822.

4 Kasivisvanathan V, Rannikko AS, Borghi M, Panebianco V, Mynderse LA, Vaarala MH, Briganti A, Budäus L, Hellawell G, Hindley RG, Roobol MJ, Eggener S, Ghei M, Villers A, Bladou F, Villeirs GM, Virdi J, Boxler S, Robert G, Singh PB, Venderink W, Hadaschik BA, Ruffion A, Hu JC, Margolis D, Crouzet S, Klotz L, Taneja SS, Pinto P, Gill I, Allen C, Giganti F, Freeman A, Morris S, Punwani S, Williams NR, Brew-Graves C, Deeks J, Takwoingi Y, Emberton M, Moore CM; PRECISION Study Group Collaborators. MRI-Targeted or Standard Biopsy for Prostate-Cancer Diagnosis. N Engl J Med. 2018 Mar 18. doi: 10.1056/NEJMoa1801993. [Epub ahead of print].

5 Barrett T, Turkbey B, Choyke PL. PI-RADS version 2: what you need to know. Clin Radiol. 2015;70(11):1165–76. doi:10.1016/j. crad.2015.06.093.

6 de Rooij M, Hamoen EH, Witjes JA, Barentsz JO, Rovers MM. Accuracy of Magnetic Resonance Imaging for Local Staging of Prostate Cancer: A Diagnostic Meta-analysis. Eur Urol. 2016 Aug;70(2):233-45.

7 Li18 Li R, Ravizzini GC, Gorin MA, Maurer T, Eiber M, Cooperberg MR, Alemozzaffar M, Tollefson MK, Delacroix SE, Chapin BF. The use of PET/CT in prostate cancer. Prostate Cancer Prostatic Dis. 2018 Apr;21(1):4-21.

8 Roach PJ, Francis R, Emmett L, Hsiao E, Kneebone A, Hruby G, Eade T, Nguyen QA, Thompson BD, Cusick T, McCarthy M, Tang C, Ho B, Stricker PD, Scott AM. The Impact of 68Ga-PSMA PET/CT on Management Intent in Prostate Cancer: Results of an Australian Prospective Multicenter Study. J Nucl Med. 2018 Jan;59(1):82-88.

9 Afaq A, Alahmed S, Chen SH, Lengana T, Haroon A, Payne H, Ahmed H, Punwani S, Sathekge M, Bomanji J. Impact of 68Ga-Prostate-Specific Membrane Antigen PET/CT on Prostate Cancer Management. J Nucl Med. 2018 Jan;59(1):89-92.

10 Freitag MT, Radtke JP, Afshar-Oromieh A, Roethke MC, Hadaschik BA, Gleave M, et al. Local recurrence of prostate cancer after radical prostatectomy is at risk to be missed in (68)Ga-PSMA- 11-PET of PET/CT and PET/MRI: comparison with mpMRI inte- grated in simultaneous PET/MRI. Eur J Nucl Med Mol Imaging. 2017;44:776–87.

11 Eiber M, Weirich G, Holzapfel K, Souvatzoglou M, Haller B, Rauscher I, et al. Simultaneous 68Ga-PSMA HBED-CC PET/MRI improves the localization of primary prostate cancer. Eur Urol. 2016;70:829–36.

12 Freitag MT, Kesch C, Cardinale J, Flechsig P, Floca R, Eiber M, Bonekamp D, Radtke JP, Kratochwil C, Kopka K, Hohenfellner M, Stenzinger A, Schlemmer HP, Haberkorn U, Giesel F. Simultaneous whole-body 18F-PSMA-1007-PET/MRI with integrated high-resolution multiparametric imaging of the prostatic fossa for comprehensive oncological staging of patients with prostate cancer: a pilot study. Eur J Nucl Med Mol Imaging. 2018 Mar;45(3):340-347.

13 Lütje S, Blex S, Gomez B, Schaarschmidt BM, Umutlu L, Forsting M, Jentzen W, Bockisch A, Poeppel TD, Wetter A. Optimization of Acquisition time of 68Ga-PSMA-Ligand PET/MRI in Patients with Local and Metastatic Prostate Cancer. PLoS One. 2016 Oct 18;11(10):e0164392. doi: 10.1371/journal.pone.0164392.

14 Giesel FL, Sterzing F, Schlemmer HP, Holland-Letz T, Mier W, Rius M, Afshar-Oromieh A, Kopka K, Debus J, Haberkorn U, Kratochwil C. Intra-individual comparison of (68)Ga-PSMA-11-PET/CT and multi-parametric MR for imaging of primary prostate cancer. Eur J Nucl Med Mol Imaging. 2016 Jul;43(8):1400-6.

Contact

Professor Heinz-Peter Schlemmer, M.D., Ph.D.
German Cancer Research Center – DKFZ
Director of the Division of Radiology (E010)
Coordinator of the Research Topic Imaging and Radiooncology
Im Neuenheimer Feld 280
69120 Heidelberg
Tel.: +49 6221 42 2563
h.schlemmer@dkfz.de

Combined ^{18}F-FDG MR/PET for Enhanced Imaging of Active Cardiac Sarcoidosis

Maria Giovanna Trivieri, M.D., Ph.D.; Philip M. Robson, Ph.D.; Nicolas A. Karakatsanis, Ph.D., MEng; Marc R. Dweck, M.D., Ph.D.; Ronan Abgral, M.D., Ph.D.; Jason C. Kovacic, M.D., Ph.D.; Zahi A. Fayad, Ph.D.

Translational and Molecular Imaging Institute, Icahn School of Medicine at Mount Sinai, New York, NY, USA

Introduction

Sarcoidosis is a multisystem disease or syndrome characterized by granuloma formation, inflammation, and fibrosis most commonly affecting the lungs and mediastinal lymph nodes [1]. Cardiac involvement is under-diagnosed but is the leading cause of death amongst patients with sarcoidosis [2–6]. Early intervention with steroids appears to improve prognosis [7], making the accurate and early diagnosis of subclinical but active cardiac sarcoidosis an important clinical goal; despite that, establishing this diagnosis remains clinically challenging [8, 9]. Cardiac magnetic resonance (MR) imaging with late gadolinium enhancement (LGE) has recently gained momentum thanks to its ability to identify the classic pattern of myocardial injury due to cardiac sarcoidosis [10, 11]. However, LGE cannot differentiate between active disease and old chronic scarring, thus limiting the specificity of CMR-based active sarcoidosis assessments. On the other hand, positron emission tomography (PET) imaging with ^{18}F-Fluorodeoxyglucose (^{18}F-FDG) [1], can identify regions of increased myocardial inflammation in patients with active cardiac sarcoidosis [12–14]. However, glucose is the predominant source of energy consumed by the myocardium, and high non-specific physiological uptake of ^{18}F-FDG can often lead to false positive identification of active myocardial disease.

Simultaneous hybrid MR/PET systems such as the Biograph mMR (Siemens Healthcare, Erlangen, Germany), combine a sensitive PET scanner with a 3T MR system to enable spatial co-registration of complementary imaging data from the two modalities [20]. Simultaneous acquisition of PET and MR data allows disease activity measured by PET to be precisely overlaid on the pattern of injury in the myocardium determined by MR from a single scan session [21, 22]. Moreover, by replacing CT with MR, PET/MR is associated with a lower radiation dose, which is especially important in chronic conditions such as cardiac sarcoidosis, where follow-up would be desirable [17]. Recent studies in our institution have investigated the use of MR/PET for evaluating cardiac disease [23, 24] in patients with suspected cardiac sarcoidosis by assessing the overlap between ^{18}F-FDG PET activity and the pattern of myocardial injury on LGE MR.

Enhancing cardiac sarcoid diagnosis with simultaneous MR/PET imaging

In a study of 25 patients, we demonstrated the potential of combined MR/PET to differentiate between active and inactive cardiac sarcoid as well as identifying false-positive PET scans, resulting from inadequate physiological ^{18}F-FDG myocardial uptake suppression [25]. Patients were considered sarcoid-positive (CS+) when a region of focal ^{18}F-FDG activity co-localized with the characteristic pattern of LGE on MRI. Inactive disease was designated by characteristic LGE but no ^{18}F-FDG activity, and a false-positive study was indicated by ^{18}F-FDG uptake without the presence of LGE. Quantitative PET analysis was subsequently based on regions-of-interest (ROIs) drawn over areas of LGE. Combined MR/PET images also enabled the identification of a new quantitative parameter, the target-to-normal-myocardium ratio (TNR), obtained by normalizing ^{18}F-FDG activity in a region defined by positive LGE to one with absent LGE enhancement. Quantitative analysis demonstrated a clear benefit in using MR to guide PET analysis. Between sarcoid-positive and sarcoid-negative patient groups, TNR was significantly different unlike conventional target-to-background ratio (TBR) and standard-uptake-value (SUV) parameters. ROC-analysis showed a sensitivity, specificity, and accuracy of 100%, 94%, and 96% for combined MR/PET to predict positive cardiac sarcoid.

In this article, four clinical exams are presented where the initial diagnosis of active cardiac sarcoidosis was unclear when either LGE MR or ^{18}F-FDG PET exams were evaluated independently. The acquisition protocols used in these studies are described in Dweck et al. [25].

In patients 1 and 2, elevated ^{18}F-FDG uptake (> 60 min post tracer injection) co-localized with the pattern of LGE MR (Fig. 1). The coincidental observation of both increased ^{18}F-FDG-PET activity and evidence of myocardial injury on

LGE strongly suggests the presence of active cardiac sarcoidosis. Target-to-background (TBR) values were calculated as mean standard uptake values (SUV) in regions-of-interest (ROI) drawn over the area of myocardial injury divided by the blood pool SUV_{mean} in the left ventricular cavity. Mean ^{18}F-FDG TBR in areas of myocardial injury were 2.2 (patient 1) and 2.0 (patient 2).

Conversely, overlap of PET and LGE was not observed in patients 3 and 4 (Fig. 2). In patient 3 transmural scarring in a coronary distribution pattern involving the anteroseptum was observed on LGE MR but there was no evidence of increased ^{18}F-FDG uptake in the same region. This finding was felt to be consistent with a chronic and silent myocardial infarction. By contrast, patient 4 demonstrated avid and diffuse ^{18}F-FDG uptake throughout the entire left ventricular myocardium in the absence of evidence of myocardial injury on LGE MR. Given that cardiac sarcoidosis is a focal disease process this was felt likely to represent failed suppression of the physiological ^{18}F-FDG uptake [27]. This hypothesis was supported by the very high TBR values (6.3, 60–90 min post injection).

These promising results highlight the benefit of simultaneous PET/MR in the assessment of myocardial inflammatory diseases. Further studies are now required to be able to differentiate the true-positive from false-positive cardiac ^{18}F-FDG uptake in the absence of positive LGE MR signal.

References

1 Baughman, R.P., Teirstein, A.S., Judson, M.A., Rossman, M.D., Yeager Jr, H., Bresnitz, E.A., De Palo, L, Hunninghake, G., Iannuzzi, M.C., Johns, C.J. and McLennan, G. 2001. Clinical characteristics of patients in a case control study of sarcoidosis. Am J Resp Crit Care Med, 164(10), pp.1885-1889.

2 Kim, J.S., Judson, M.A., Donnino, R., Gold, M., Cooper, L.T., Prystowsky, E.N. and Prystowsky, S., 2009. Cardiac sarcoidosis. Am Heart J, 157(1), pp.9-21.

3 Iannuzzi, M.C. and Fontana, J.R., 2011. Sarcoidosis: clinical presentation, immunopathogenesis, and therapeutics. Jama, 305(4), pp.391-399.

4 Silverman, K.J., Hutchins, G.M. and Bulkley, B.H., 1978. Cardiac sarcoid: a clinicopathologic study of 84 unselected patients with systemic sarcoidosis.Circulation, 58(6), pp.1204-1211.

5 Hunninghake, G.W., Costabel, U., Ando, M., Baughman, R., Cordier, J.F., Du Bois, R., Eklund, A., Kitaichi, M., Lynch, J., Rizzato, G. and Rose, C., 1999. ATS/ERS/ WASOG statement on sarcoidosis. J WASOG/World Assoc Sarc Other Granul Disord, 16(2), p.149.

6 Morgenthau, A.S. and Iannuzzi, M.C., 2011. Recent advances in sarcoidosis. CHEST, 139(1), pp.174-182.

7 Uemura, A., Morimoto, S.I., Hiramitsu, S., Kato, Y., Ito, T. and Hishida, H., 1999. Histologic diagnostic rate of cardiac sarcoidosis: evaluation of endomyocardial biopsies. Am Heart J, 138(2), pp.299-302.

8 Frank, H. and Globits, S., 1999. Magnetic resonance imaging evaluation of myocardial and pericardial disease. J Mag Res Imag, 10(5), pp.617-626.

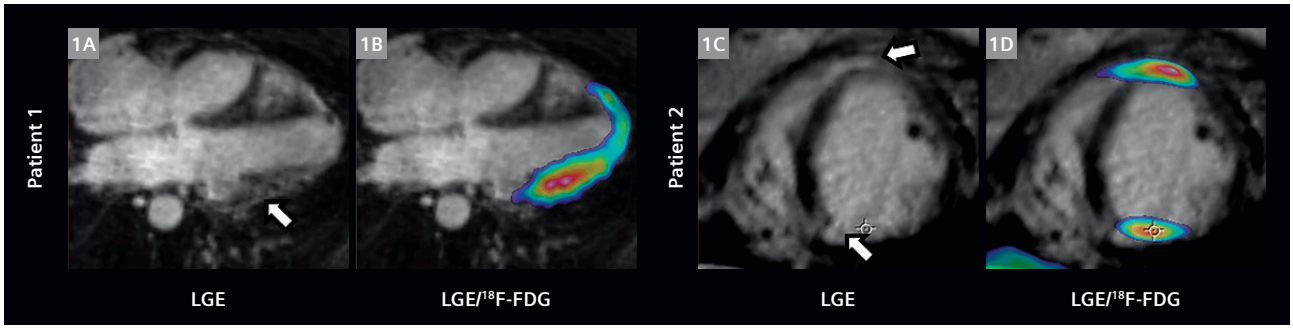

1 **From left to right: (1A, C)** LGE MR images showed elevated LGE signal at the lateral and anteroseptal wall for patient 1 (62-year-old male) and patient 2 (63-year-old female) respectively. **(1B, D)** Matched ^{18}F-FDG PET fused with previous LGE MR images showed high ^{18}F-FDG uptake overlapping with the LGE pattern of injury.

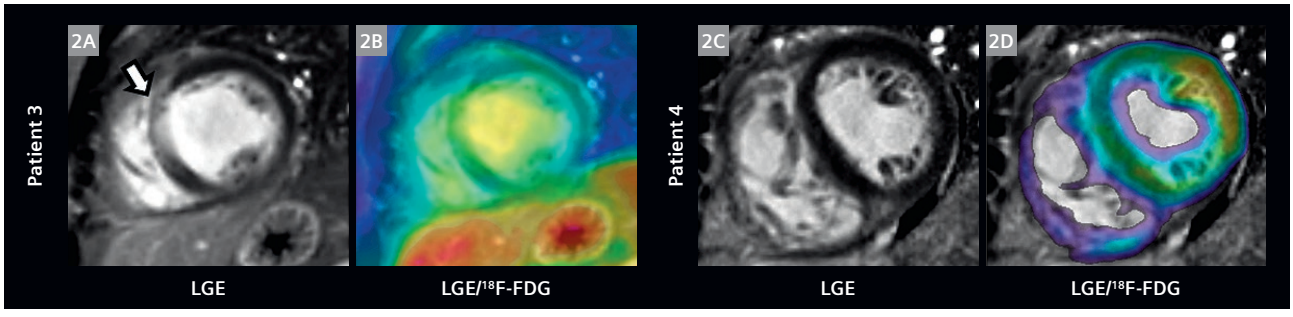

2 **(2A, B)** Patient 3 (50-year-old female), short-axis LGE MR showed transmural LGE on the anteroseptum, while fused PET/MR images demonstrated absence of high ^{18}F-FDG uptake on the same region. **(2C, D)** Patient 4 (42-year-old male) LGE MR showed absence of LGE on the myocardial wall. Fused PET/MR images indicated diffused intense ^{18}F-FDG uptake.

9 Yamagishi, H., Shirai, N., Takagi, M., Yoshiyama, M., Akioka, K., Takeuchi, K. and Yoshikawa, J., 2003. Identification of cardiac sarcoidosis with 13N-NH3/18F-FDG PET. J Nucl Med, 44(7), pp.1030-1036.
10 Patel, M.R., Cawley, P.J., Heitner, J.F., Klem, I., Parker, M.A., Jaroudi, W.A., Meine, T.J., White, J.B., Elliott, M.D., Kim, H.W., Judd, R.M., 2009. Detection of myocardial damage in patients with sarcoidosis. Circulation, 120(20), pp.1969-1977.
11 Tadamura, E., Yamamuro, M., Kubo, S., Kanao, S., Saga, T., Harada, M., Ohba, M., Hosokawa, R., Kimura, T., Kita, T. and Togashi, K., 2005. Effectiveness of delayed enhanced MRI for identification of cardiac sarcoidosis: comparison with radionuclide imaging. Am J Roentgen, 185(1), pp.110-115.
12 Youssef, G., Leung, E., Mylonas, I., Nery, P., Williams, K., Wisenberg, G., Gulenchyn, K.Y., DaSilva, J., Birnie, D., Wells, G.A. and Beanlands, R.S., 2012. The use of 18F-FDG PET in the diagnosis of cardiac sarcoidosis: a systematic review and metaanalysis including the Ontario experience. J Nucl Med, 53(2), pp.241-248.
13 Soussan, M., Augier, A., Brillet, P.Y., Weinmann, P. and Valeyre, D., 2014. Functional imaging in extrapulmonary sarcoidosis: FDG-PET/CT and MR features. Clin Nucl Med, 39(2), pp.e146-e159.
14 Manabe, O., Yoshinaga, K., Ohira, H. and Oyama-Manabe, N., 2016. Usefulness of 18F-FDG PET in Diagnosing Cardiac Sarcoidosis. InPerspectives on Nuclear Medicine for Molecular Diagnosis and Integrated Therapy (pp. 209-216). Springer Japan.
17 Pichler, B.J., Kolb, A., Nagele, T. and Schlemmer, H.P., 2010. PET/MRI: paving the way for the next generation of clinical multimodality imaging applications. J Nucl Med, 51(3), pp.333-336
20 Delso, G., Furst, S., Jakoby, B., Ladebeck, R., Ganter, C., Nekolla, S.G., Schwaiger, M. and Ziegler, S.I., 2011. Performance measurements of the Siemens mMR integrated whole-body PET/MR scanner. J Nucl Med, 52(12), pp.1914-1922
21 Schneider, S., Batrice, A., Rischpler, C., Eiber, M., Ibrahim, T. and Nekolla, S.G., 2014. Utility of multimodal cardiac imaging with PET/MRI in cardiac sarcoidosis: implications for diagnosis, monitoring and treatment. Eur Heart J, 35(5), pp.312-312.
22 White J.A., Rajchl M., Butler J., Thompson, R.T., Prato, F.S., Wisenberg G., 2013. "Active cardiac sarcoidosis: first clinical experience of simultaneous positron emission tomography-magnetic resonance imaging for the diagnosis of cardiac disease." Circulation. 2013, 127 (22) p. e639-e641.
23 Abgral, R., Dweck, M.R., Robson, P.M., Trivieri, M.G., Karakatsanis, N.A., Sanz, J., Contreras, J., Fuster, V., Padilla, M., Kovacic, J.C. and Fayad, Z.A., 2016. Usefulness of combined FDG-PET/MR to diagnose active cardiac sarcoidosis. J Nucl Med, 57(suppl 2), pp.1668-1668.
24 Abgral, R., Dweck, M.R., Robson, P.M., Trivieri, M.G., Karakatsanis, N.A., Mani, V., Padilla, M., Miller, M., Lala, A., Sanz, J., Narula, J., Fuster, V., Contreras, J., Kovacic, J.C. and Fayad, Z.A., 2016. Clinical Utility of Combined FDG-PET/MR to Assess Myocardial Disease. JACC Cardiovasc Imaging. 2017 May;10(5):594-597
25 Dweck R.M., Abgral R., Trivieri M.G., Robson P.M. Karakatsanis N., Mani V., Palmisano A., Miller M.A., Lala A., Chang H.L., Sanz J., Contreras J., Narula J., Fuster V., Padilla M., Fayad Z.A., Kovacic J.C., 2018. Hybrid Magnetic Resonance Imaging and Positron Emission Tomography With Fluorodeoxyglucose to Diagnose Active Cardiac Sarcoidosis. JACC: Cardiovascular Imaging. 11 (1), p. 94 - 107.
26 Karakatsanis N.A., Dweck M.R., Abgral R., Trivieri, M.G., Robson P.M., Kovacic J.C., Fayad Z.A., 2018. Combined 18F-FDG PET/MR for Enhanced Imaging of Active Cardiac Sarcoidosis. MAGNETOM Flash 67 (1) pp.34-36
27 Williams, G. and Kolodny, G.M., 2008. Suppression of myocardial 18F-FDG uptake by preparing patients with a high-fat, lowcarbohydrate diet. Am J Roentg, 190(2), pp.W151-W156

Further Reading

1 Dweck R.M., Abgral R., Trivieri M.G., Robson P.M. Karakatsanis N., Mani V., Palmisano A., Miller M.A., Lala A., Chang H.L., Sanz J., Contreras J., Narula J., Fuster V., Padilla M., Fayad Z.A., Kovacic J.C., 2018. "Hybrid Magnetic Resonance Imaging and Positron Emission Tomography With Fluorodeoxyglucose to Diagnose Active Cardiac Sarcoidosis". JACC: Cardiovascular Imaging. 11 (1), p. 94 - 107.
2 Wicks E.C., Menezes L.J., Barnes A., Mohiddin S.A., Sekhri N., Porter J.C., Booth H.L. Garrett E., Patel R.S., Pavlou M., Groves A.M., Elliott P.M., 2018. "Diagnostic accuracy and prognostic value of simultaneous hybrid 18F-fluorodeoxyglucose positron emission tomography/magnetic resonance imaging in cardiac sarcoidosis". European Heart Journal - Cardiovascular Imaging, Jan 8. doi: 10.1093/ehjci/jex340. PubMed PMID: 29319785.
3 Ferda, J., Hromadka, M., Baxa, J., 2016. "Imaging of the myocardium using 18F-FDG-PET/MRI". E J of Rad. 85, p. 1900-1908.
4 Nensa, F., Tezgah, E., Poeppel, T., Nassenstein, K., Schlosser, T., 2016. "Feasibility of FDG-PET in myocarditis: Comparison to CMR using integrated PET/MRI". Journal of Nuclear Cardiology., DOI: 10.1007/s12350-016-0616-y.
5 Nensa, F., Tezgah, E., Poeppel, T., Nassenstein, K., Schlosser, T., 2015. "Diagnosis and treatment response evaluation of cardiac sarcoidosis using positron emission tomography/magnetic resonance imaging". Eur Heart J. 36 (9) p. 550.
6 O'Meara, C., Menezes, L.J. White, S.K., Wicks, E., Perry E., 2013. "Inital experience of imaging cardiac sarcoidosis using hybrid PET-MR - a technologist's case study". J Cardiovasc Magn Reson. 15 (1) p. 1-2.
7 Schneider S., Batrice A., Rischpler C., Eiber M., Ibrahim, T., Nekolla, S.G., 2013. "Utility of multimodal cardiac imaging with PET/MRI in cardiac sarcoidosis: implications for diagnosis, monitoring and treatment.". Eur Heart J.35, p. 312.
8 White J.A., Rajchl M., Butler J., Thompson, R.T., Prato, F.S., Wisenberg G., 2013. "Active cardiac sarcoidosis: first clinical experience of simultaneous positron emission tomography-magnetic resonance imaging for the diagnosis of cardiac disease." Circulation. 2013, 127 (22) p. e639--e641.

Contact

Zahi A. Fayad, Ph.D., FAHA, FACC, FISMRM
Icahn School of Medicine at Mount Sinai
Mount Sinai Endowed Chair in Medical Imaging and Bioengineering
Professor of Radiology and Medicine (Cardiology), Director, Translational and Molecular Imaging Institute
Director, Cardiovascular Imaging Research, Vice-Chair for Research, Department of Radiology
One Gustave L. Levy Place, Box 1234
New York, NY 10029-6574
USA
Phone: +1 212 824 8452, Fax: +1 240 368 8096
zahi.fayad@mssm.edu

MR/PET: Nuts and Bolts for Abdominal Imaging

Lillian Xiong[1], Debra Gervais[1], Bruce R. Rosen[1], David Groshar[2], Lina Garcia Canamaque[3], Hanna Bernstine[2], Tiffany Ting-Fang Shih[4], Ken Hermann[5], Lale Umutlu[5], Onofrio A. Catalano[1, 6]

[1] Massachusetts General Hospital, Harvard Medical School, Boston, MA, USA
[2] Assuta Medical Center and Rabin Medical Center, Sackler Faculty of Medicine, Tel Aviv, Israel
[3] HM Hospitales Sanchinarro and Puerta del Sur, Hospital Universitario Madrid Sanchinarro, Madrid, Spain
[4] National Taiwan University Hospital, National Taiwan University, Taipei, Taiwan
[5] University Hospital Essen, University of Duisburg-Essen, Essen, Germany
[6] University of Naples Parthenope, Naples, Italy

Introduction

PET/CT is currently the gold standard for staging several solid organ neoplasms and has been shown to be more accurate in TNM staging than CT or PET alone [1, 2]. Additionally, quantification of radiotracer uptake is helpful in assessing treatment response by evaluating changes in lesion metabolism [3, 4].

MR/PET is a hybrid imaging technique that acquires and fuses anatomic and functional data from magnetic resonance (MR) and metabolic information from positron emission tomography (PET) [5, 6]. There are many potential advantages over PET/CT as well as over stand-alone MR and PET for oncological imaging. Simultaneous acquisition of the MR and PET with the resultant direct spatial and temporal matching of MR and PET data allows for motion correcting both MR and PET data, leading to improved image quality, increased detection rates, and more precise quantitation of lesion pharmacokinetics and metabolism, including standard uptake values (SUV) and metabolic tumor volume (MTV) [5, 7, 8].

Benefits of MR/PET

Both MR/PET and PET/CT take advantage of the high sensitivity typical of PET. In fact, PET can detect metabolically active lesions harboring cell populations at least 2–3 order of magnitude less than CT or MR (10^7 cells/lesion versus 10^{10} cells/lesion).

However, PET/CT performance has limitations related to the low soft tissue signal to noise ratio of CT and the sequential acquisition of CT and PET data, leading to poor lesion allocation in certain anatomic regions and in the case of small size [9–11].

MR exhibits higher soft tissue signal to noise ratio than CT and is also capable of providing functional information through diffusion-weighted imaging (DWI). DWI explores lesion cellularity and can be used for detecting hypercellular neoplasms regardless of their glucose metabolism, making DWI appealing for investigating neoplasms that might not be particularly FDG avid, like well-differentiated hepatocellular carcinoma, mucinous adenocarcinomas, well differentiated neuroendocrine tumors and some low-grade lymphomas [12, 13].

MR/PET, bringing to the table the full potentialities of both MR and PET, has several potential advantages over PET/CT. First, the possibility to simultaneously acquire MR and PET data makes co-registration and fusion of MR and PET more robust and accurate than by PET/CT; moreover, the co-acquisition of MR and PET allows to compensate for motion both MR and PET in ways that can be implemented in the routine clinical practice. Then the superior anatomic layout of MR produces images with more diagnostic information and improved details, that might provide anatomic correlates for areas of increased metabolism. These features, unique to MR/PET, allow for better detection of anatomic primary and metastatic disease within the abdomen and pelvis [7, 14, 15]. Moreover, the combination of morpho-functional MR criteria (including DWI and ADC values) and the metabolic PET criteria may lead to increased specificity and improved readers' confidence [16, 17]. In our experience, the superior ability of MR/PET to characterize sub-centimeter lesions as benign or malignant is responsible for increased staging accuracy over other modalities like PET/CT, and stand-alone MR.

Rectal cancer

The higher soft tissue signal to noise ratio of MR, as compared to CT, accounts for improved depiction of fine anatomic details in MR/PET, when compared to PET/CT [5, 18, 19]. In the case of rectal cancer, this might allow for clearer depiction of lesion margins, local tumor infiltration, and relationships of lesions to adjacent structures, evaluation of extension beyond the tunica muscularis and distance from the mesorectal fascia. In cases of rectal cancer, up to 15% of pelvic lymph nodes less than 5 mm are metastatic [20]. MR-based morpho-functional indices such as lymph node T2-weighted characteristics, internal structure, shape, margins, and ADC value (ADC < 1.0 x 10^{-3} mm^2/s suggesting malignancy in our experience), combined with metabolic PET data account for good performance figures of MR/PET in the assessment of lymph nodes. Moreover, the joined assessment of the PET and MR data may provide insight into biology of lymphadenopathy that might be difficult to achieve by each of them standing alone (Figures 1, 2).

Gynecologic cancers

PET/CT imaging is limited when it comes to local staging of pelvic cancers due to the low soft tissue contrast and the presence of excreted radiotracer in the bladder that interferes with the assessment of adjacent structures [21]. MR alone is also limited, given the potentiality for metastatic disease in lymph nodes < 10 mm, a limitation previously discussed in cases of rectal cancer. MR/PET combines the improved T staging from the high soft tissue contrastof of MR, with the high N staging of MR plus PET [22, 23]. Furthermore, the low sensitivity of MR for the detection of small peritoneal implants and recurrent/residual disease after treatment may take advantage of the concurrent PET [22–24]. From the published literature and our initial experience, we feel that MR/PET will prove superior to MR or PET alone in both initial staging of gynecologic cancers and post treatment surveillance.

Liver

MR alone is far superior to CT in evaluating the liver parenchyma and in characterizing lesions. Moreover, differently from CT, hepatic assessment is not limited by hepatic steatosis, often a side effect of chemotherapy. PET improves the detection and characterization of lesions adjacent to the capsule and to the intrahepatic vasculature. Additionally, PET helps evaluate areas that have undergone local regional therapies (i.e., TACE, thermal ablation, and SIRT) [25–27]. Preliminary clinical studies suggest that MR/PET overcomes PET/CT and hepatospecific contrast enhanced MRI in the case of < 10 mm hepatic metastases and in patients who underwent chemotherapy. In initial studies this translated in detecting liver lesions in 6% of cases otherwise deemed free of hepatic metastases [28–30].

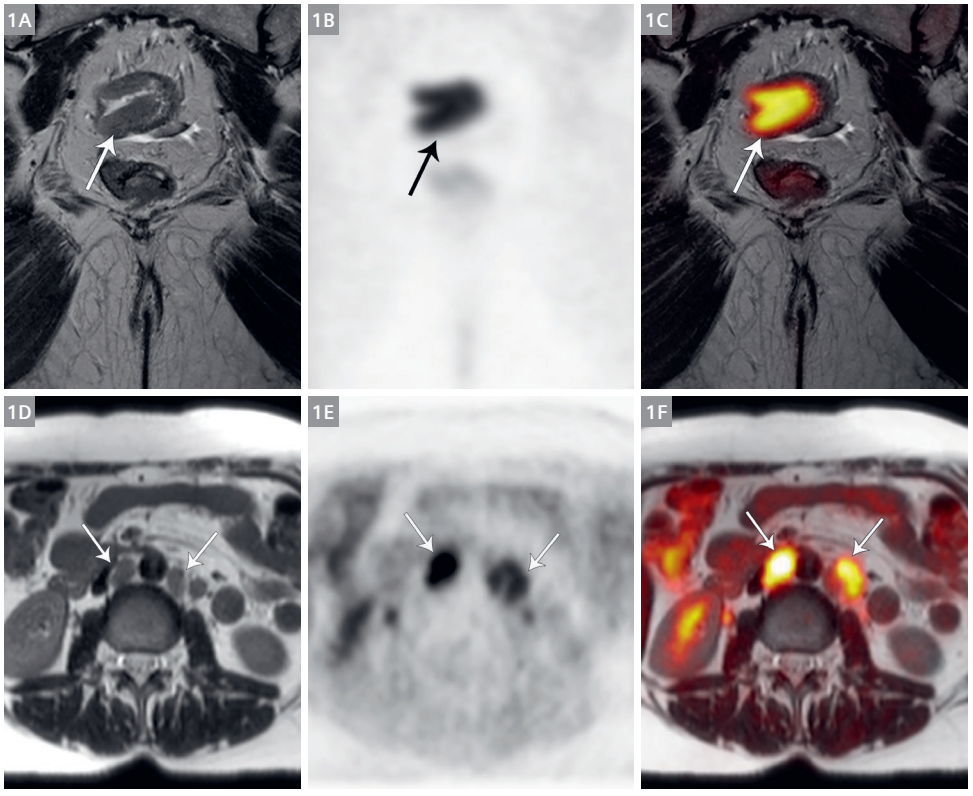

1 Rectal cancer. Pelvic coronal T2w FSE **(1A)**, coronal PET **(1B)**, fused MR/PET **(1C)**; mid abdominal axial T2w SSFSE **(1D)**, axial PET **(1E)**, and fused MR/PET **(1F)**. Primary cancer is indicated by arrow in 1A–C, retroperitoneal lymphadenopathy by arrows in 1D–E. MR/PET allows to ascertain the integrity of the tunica muscularis in 1A. Note correspondence of the morphologic and metabolic abnormalities in the primary rectal cancer. The retroperitoneal metastatic lymph nodes demonstrate increased FDG uptake, similarly to the primary cancer, indistinct margins, intermediate and heterogeneous signal intensity and loss of the central hilum.

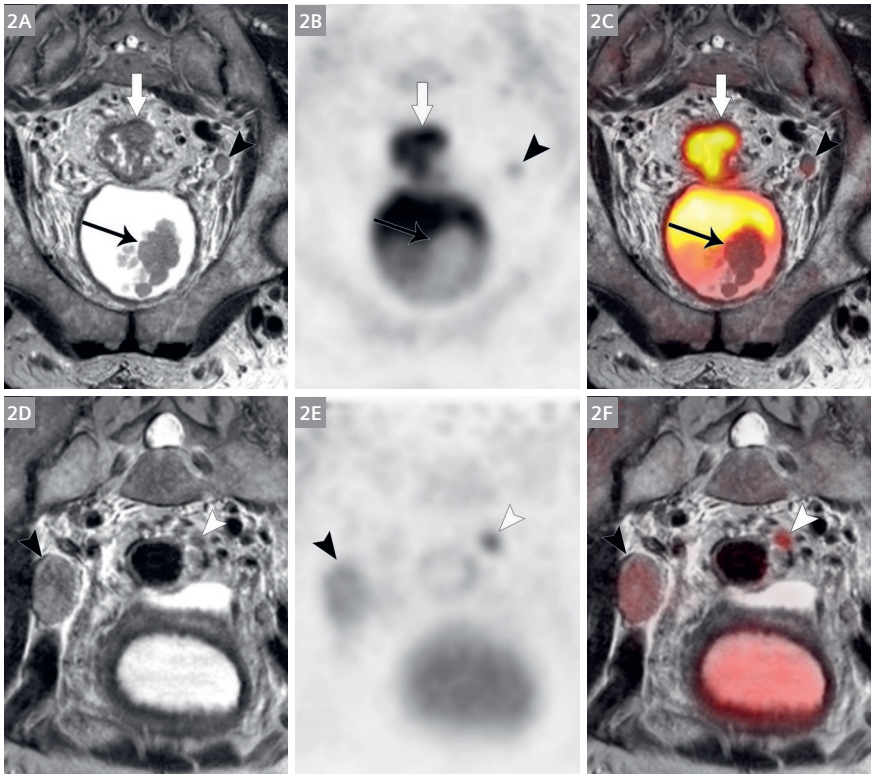

2 Rectal cancer and prostate cancer.
Pelvic coronal T2w FSE **(2A, D)**, coronal PET **(2B, E)**, fused MR/PET **(2C, F)**.
Primary rectal cancer indicated by thick white arrow. Prostate cancer infiltrating and growing within the bladder is indicated by thin black arrow.
Primary rectal cancer is markedly FDG avid, meanwhile primary prostate cancer is not. Mesorectal lymphadenopathy (white arrowhead in 2D–F), despite its small size, exhibits medium FDG uptake, as well as internal structural heterogeneity.
It was biopsied and proven to be metastatic from rectal cancer.
The large and heterogeneous right and left pelvic side wall lymphadenopathy (black arrowheads in 2A–F) are FDG negative and biopsy proven metastatic from prostate cancer.
Despite the morphologic similarities, the very different FDG uptake between the mesorectal and the pelvic side wall lymphadenopathy alerted about a possible different biology that translated in differences in TNM staging.

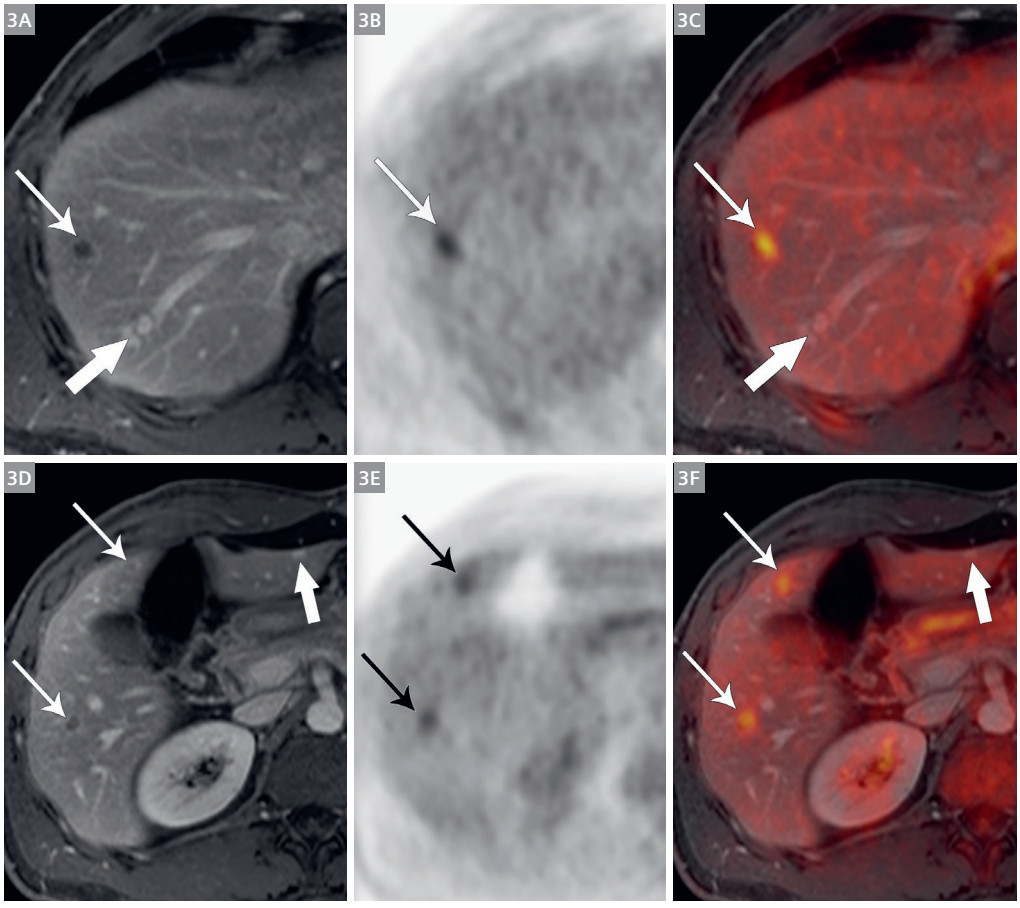

3 Liver metastases from colon cancer.
Axial T1w portal venous phase VIBE **(3A, D)**, axial PET **(3B, E)**, fused MR/PET **(3C, F)**.
A rind of peripheral enhancement and marked FDG uptake allow to characterize the liver metastases (thin arrows) as such even when small, as in 3D–F.
On the other hand, lack of FDG uptake, globular enhancement in 3A, homogeneous enhancement in 3D, and enhancement paralleling that of the blood stream allow the coexisting hemangiomas (thick arrows) to be characterized as such, even when very small as in 3F.

Osseous structures
When exploring the abdomen and pelvis, its mandatory to carefully assess for bony metastases. Most sclerotic lesions are easily detected by CT, however subtle lytic and even some sclerotic lesions can be overlooked. Furthermore, the evaluation for osseous metastatic disease is limited in patients with osteopenia on CT. PET uptake is confounded in the setting of increased hematopoietic bone marrow uptake from chemotherapy or colony stimulating factor administration and thus limits evaluation of osseous metastatic disease [31–33]. MR allows for detection of subtle marrow changes. In a comparative study, it has been shown that whole-body MR outperforms bone scintigraphy and targeted X-rays, being more sensitive for bone metastases from prostate cancer (sensitivity of 98–100% versus 86% respectively). However, whole-body MR had similar specificity (specificity of 98–100% versus 98% respectively) [33]. In a dedicated study comparing FDG-PET/CT versus FDG-PET/MR in assessing for bone metastases in breast cancer patients, MR/PET disclosed metastases in 12% more patients than PET/CT [15].

Pitfalls

Many factors have the potential to hamper MR/PET performance, like image degradation due to magnetic susceptibility artifacts or eddy currents. Motion/breathing artifacts causing image blurring, poor localization of metabolically avid lesions (particularly in the region of the diaphragm, heart, and bowel), over-estimation of MTV, and underestimation of SUV are challenging both in PET/CT and in MR/PET. However, while they are very difficult to resolve in PET/CT, some approaches have been successfully developed to address them in MR/PET, like BodyCompass and a novel self-navigated method developed at our institution [8]. Therefore, motion/breathing artifacts are less challenging in state of the art MR/PET scanners. MR/PET requires appropriate patient cooperation and is a longer examination than PET/CT (average length 50–80 minutes for a whole-body protocol MR/PET versus 15–20 minutes for a whole-body protocol PET/CT), therefore not all patients are fit for its lengthier acquisition time.

Conclusion

MR/PET has many advantages over the other imaging modalities when evaluating primary malignancies and metastases within the abdomen and pelvis. Simultaneous MR and PET imaging allows for less miss-registration and improved detection of small lesions. The superior soft tissue contrast provided by MRI allows characterization and detection of lesions that are not readily evident by CT. The PET portion of the examination provides metabolic information that improves reader confidence and helps distinguish between treatment changes and recurrent/residual diseases in cases of treated malignancies. These advantages are most evident in regard to lymph node involvement, liver, bone, and pelvic organs.

Suggested readings

- PET/MR Imaging: Current and Emerging Applications, Lale Umutlu and Ken Herrmann, Springer 2018.
- Principles of PET/MR Imaging. Disselhorst JA, Bezrukov I, Kolb A, Parl C, Pichler BJ. J Nucl Med. 2014 Jun 1;55(Supplement 2):2S-10S. Epub 2014 May 12.
- Comparison of 18F-FDG-PET/CT and 18F-FDG-PET/MR imaging in oncology: a systematic review. Singnurkar A, Poon R, Metser U. Ann Nucl Med. 2017 Jun;31(5):366-378. doi: 10.1007/s12149-017-1164-5. Epub 2017 Mar 28.
- PET/MR imaging of pelvic malignancies. Wetter A, Grueneisen J, Umutlu L. Eur J Radiol. 2017 Sep;94: A44-A51. doi: 10.1016/j.ejrad.2017.02.026. Epub 2017 Feb 20.

References

1 Antoch G, Stattaus J, Nemat AT, et al. Non-small cell lung cancer: dual-modality PET/CT in preoperative staging. Radiology. 2003;229(2):526-533. doi:10.1148/radiol.2292021598
2 Lardinois D, Weder W, Hany TF, et al. Staging of non-small-cell lung cancer with integrated positron-emission tomography and computed tomography. N Engl J Med. 2003;348(25):2500-2507. doi:10.1056/NEJMoa022136
3 Boss DS, Olmos RV, Sinaasappel M, Beijnen JH, Schellens JHM. Application of PET/CT in the development of novel anticancer drugs. Oncologist. 2008;13(1):25-38. doi:10.1634/theoncologist.2007-0097
4 Al-Sugair A, Coleman RE. Applications of PET in lung cancer. Semin Nucl Med. 1998;28(4):303-319. http://www.ncbi.nlm.nih.gov/pubmed/9800237. Accessed July 12, 2018.
5 Delso G, Fürst S, Jakoby B, et al. Performance measurements of the Siemens mMR integrated whole-body PET/MR scanner. J Nucl Med. 2011;52(12):1914-1922. doi:10.2967/jnumed.111.092726
6 Zaidi H, Ojha N, Morich M, et al. Design and performance evaluation of a whole-body Ingenuity TF PET-MRI system. Phys Med Biol. 2011;56(10):3091-3106. doi:10.1088/0031-9155/56/10/013
7 Catalano OA, Masch WR, Catana C, et al. An overview of PET/MR, focused on clinical applications. Abdom Radiol. 2017;42(2): 631-644. doi:10.1007/s00261-016-0894-5

8 Catalano OA, Umutlu L, Fuin N, et al. Comparison of the clinical performance of upper abdominal PET/DCE-MRI with and without concurrent respiratory motion correction (MoCo). Eur J Nucl Med Mol Imaging. July 2018. doi:10.1007/s00259-018-4084-2

9 De Iaco P, Musto A, Orazi L, et al. FDG-PET/CT in advanced ovarian cancer staging: Value and pitfalls in detecting lesions in different abdominal and pelvic quadrants compared with laparoscopy. Eur J Radiol. 2011;80(2):e98-e103. doi:10.1016/j.ejrad.2010.07.013

10 Soussan M, Des Guetz G, Barrau V, et al. Comparison of FDG-PET/CT and MR with diffusion-weighted imaging for assessing peritoneal carcinomatosis from gastrointestinal malignancy. Eur Radiol. 2012;22(7):1479-1487. doi:10.1007/s00330-012-2397-2

11 De Gaetano AM, Calcagni ML, Rufini V, Valenza V, Giordano A, Bonomo L. Imaging of peritoneal carcinomatosis with FDG PET-CT: diagnostic patterns, case examples and pitfalls. Abdom Imaging. 2009;34(3):391-402. doi:10.1007/s00261-008-9405-7

12 Padhani AR, Koh D-M, Collins DJ. Whole-body diffusion-weighted MR imaging in cancer: current status and research directions. Radiology. 2011;261(3):700-718. doi:10.1148/radiol.11110474

13 Bruegel M, Holzapfel K, Gaa J, et al. Characterization of focal liver lesions by ADC measurements using a respiratory triggered diffusion-weighted single-shot echo-planar MR imaging technique. Eur Radiol. 2008;18(3):477-485. doi:10.1007/s00330-007-0785-9

14 Fornasa F, Nesoti MV, Bovo C, Bonavina MG. Diffusion-weighted magnetic resonance imaging in the characterization of axillary lymph nodes in patients with breast cancer. J Magn Reson Imaging. 2012;36(4):858-864. doi:10.1002/jmri.23706

15 Eiber M, Beer AJ, Holzapfel K, et al. Preliminary results for characterization of pelvic lymph nodes in patients with prostate cancer by diffusion-weighted MR-imaging. Invest Radiol. 2010;45(1):15-23. doi:10.1097/RLI.0b013e3181bbdc2f

16 von Schulthess GK, Schlemmer H-PW. A look ahead: PET/MR versus PET/CT. Eur J Nucl Med Mol Imaging. 2009;36 Suppl 1(S1):S3-9. doi:10.1007/s00259-008-0940-9

17 Torigian DA, Zaidi H, Kwee TC, et al. PET/MR imaging: technical aspects and potential clinical applications. Radiology. 2013;267(1):26-44. doi:10.1148/radiol.13121038

18 Brown G, Richards CJ, Bourne MW, et al. Morphologic predictors of lymph node status in rectal cancer with use of high-spatial-resolution MR imaging with histopathologic comparison. Radiology. 2003;227(2):371-377. doi:10.1148/radiol.2272011747

19 Schöder H, Larson SM. Positron emission tomography for prostate, bladder, and renal cancer. Semin Nucl Med. 2004;34(4):274-292. http://www.ncbi.nlm.nih.gov/pubmed/15493005. Accessed July 12, 2018.

20 Kim DJ, Kim JH, Ryu YH, Jeon TJ, Yu J-S, Chung J-J. Nodal staging of rectal cancer: high-resolution pelvic MRI versus 18F-FDGPET/CT. J Comput Assist Tomogr. 2011;35(5):531-534. doi:10.1097/RCT.0b013e318225720f

21 Kim SH, Choi BI, Han JK, et al. Preoperative staging of uterine cervical carcinoma: comparison of CT and MRI in 99 patients. J Comput Assist Tomogr. 17(4):633-640. http://www.ncbi.nlm.nih.gov/pubmed/8331236. Accessed July 12, 2018.

22 Kim DJ, Kim JH, Lim JS, et al. Restaging of Rectal Cancer with MR Imaging after Concurrent Chemotherapy and Radiation Therapy. RadioGraphics. 2010;30(2):503-516. doi:10.1148/rg.302095046

23 Park JM, Kim IY, Kim SW, et al. A comparative study of FDG PET/CT and enhanced multi-detector CT for detecting liver metastasis according to the size and location. Ann Nucl Med. 2013;27(3):217-224. doi:10.1007/s12149-012-0677-1

24 Holalkere N-S, Sahani D V, Blake MA, Halpern EF, Hahn PF, Mueller PR. Characterization of small liver lesions: Added role of MR after MDCT. J Comput Assist Tomogr. 30(4):591-596. http://www.ncbi.nlm.nih.gov/pubmed/16845289. Accessed July 12, 2018.

25 Barker DW, Zagoria RJ, Morton KA, Kavanagh P V, Shen P. Evaluation of liver metastases after radiofrequency ablation: utility of 18F-FDG PET and PET/CT. AJR Am J Roentgenol. 2005;184(4):1096-1102. doi:10.2214/ajr.184.4.01841096

26 Nakai T, Okuyama C, Kubota T, et al. Pitfalls of FDG-PET for the diagnosis of osteoblastic bone metastases in patients with breast cancer. Eur J Nucl Med Mol Imaging. 2005;32(11):1253-1258. doi:10.1007/s00259-005-1842-8

27 Hamaoka T, Madewell JE, Podoloff DA, Hortobagyi GN, Ueno NT. Bone Imaging in Metastatic Breast Cancer. J Clin Oncol. 2004;22(14):2942-2953. doi:10.1200/JCO.2004.08.181

28 Sugawara Y, Fisher SJ, Zasadny KR, Kison P V, Baker LH, Wahl RL. Preclinical and clinical studies of bone marrow uptake of fluorine-1-fluorodeoxyglucose with or without granulocyte colony-stimulating factor during chemotherapy. J Clin Oncol. 1998;16(1):173-180. doi:10.1200/JCO.1998.16.1.173

29 Lecouvet FE, El Mouedden J, Collette L, et al. Can whole-body magnetic resonance imaging with diffusion-weighted imaging replace Tc 99m bone scanning and computed tomography for single-step detection of metastases in patients with high-risk prostate cancer? Eur Urol. 2012;62(1):68-75. doi:10.1016/j.eururo.2012.02.020

30 Catalano OA, Nicolai E, Rosen BR, et al. Comparison of CE-FDG-PET/CT with CE-FDG-PET/MR in the evaluation of osseous metastases in breast cancer patients. Br J Cancer. 2015;112(9):1452-1460. doi:10.1038/bjc.2015.112

Contact

Onofrio A. Catalano, M.D., Ph.D.
Athinoula A. Martinos Center
for Biomedical Imaging
Massachusetts General Hospital
Harvard Medical School
Boston, MA
USA
Tel.: +1 617 643 7920
ocatalano@mgh.harvard.edu

Lale Umutlu, M.D.
University Hospital Essen
Diagnostic and interventional Radiology
and Neuroradiology
Hufelandstr. 55
45147 Essen
Germany
lale.umutlu@uk-essen.de

Hybrid Brain MR/PET Imaging in Mild Cognitive Impairment and Dementia

Solveig Tiepolt[1]; Karl-Titus Hoffmann[2]; Henryk Barthel[1]; Osama Sabri[1]

[1] Department of Nuclear Medicine, University of Leipzig, Germany
[2] Department of Neuroradiology, University of Leipzig, Germany

Introduction

Current research diagnostic criteria for Alzheimer's disease (AD) and mild cognitive impairment (MCI) implement biomarker information to improve the diagnostic certainty [1–3]. Biomarkers of the AD pathophysiological process are amyloid-β (Aβ) positron emission tomography (PET) and measurement of $A\beta_{42}$ in the cerebrospinal fluid (CSF). Biomarkers of neuronal injury are [^{18}F]fluorodeoxyglucose (FDG) PET, measurement of total tau and phosphorylated tau in CSF and structural magnetic resonance imaging (MRI) [3].

Benefits of hybrid MR/PET imaging

Using a hybrid MR/PET system, AD biomarker information can be gathered in one session which simplifies the diagnostic process and improves the patients and referrer convenience [4]. For example, using an Aβ PET radiotracer at an MR/PET system, the examination provides biomarker information on neuronal injury (structural MR) and AD pathology (late after administration Aβ PET images). An extension of the imaging protocol enables to acquire early after administration Aβ PET images that serve as FDG surrogate and provide further biomarker information on neuronal injury [5].

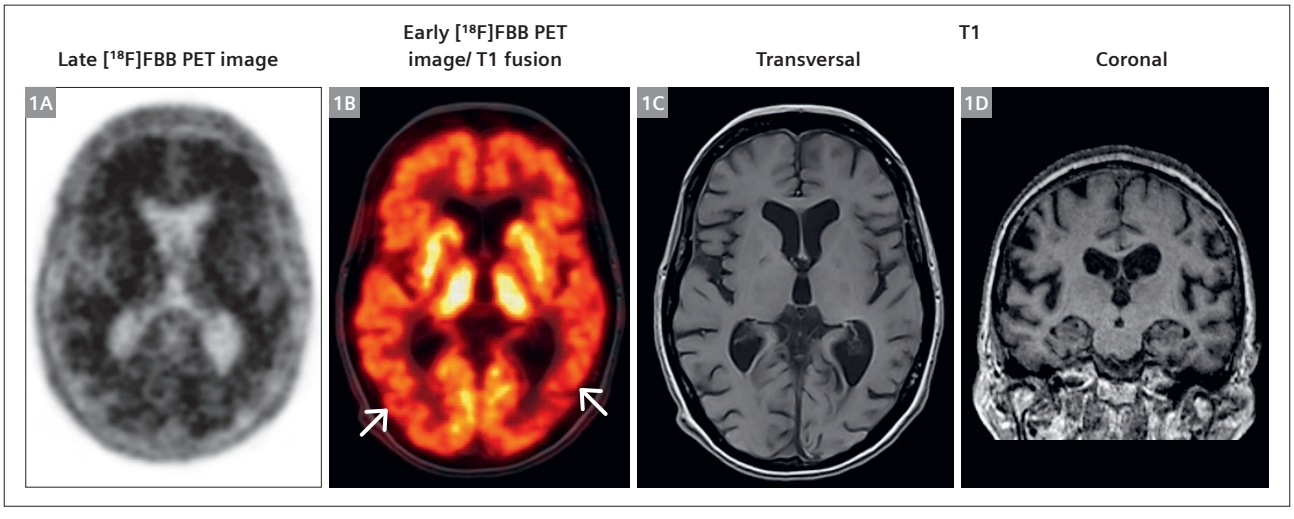

1 **[^{18}F]florbetaben (FBB) amyloid PET/MR images of a subject with mild cognitive impairment.**
(1A) shows representative images of the late after administration (90–110 min p.i.) [^{18}F]FBB PET, rendering this case amyloid-positive, **(1B)** shows representative images of the early after administration (0–10 min p.i.) [^{18}F]FBB PET fusion with the T1 map – white arrows mark reduced tracer uptake in both temporoparietal regions, **(1C, D)** show representative transversal and coronal slices of the structural T1 MR sequence. Note that the medial temporal lobe did not show signs of atrophy yet in this early AD case.

Case example from our clinical routine work

80-year-old female with mild cognitive impairment (MCI) and depressive episodes. Since two years, deficits of the short-term memory and orientation. Mini Mental State Examination (MMSE) score: 28/30. Wechsler-Memory-Scale Revised (WMS-R) immediate recall: 15 (norm > 19), delayed recall: 4 (norm > 15). Clinical diagnosis: early AD. Secondary diagnosis: depressive disorder. The patient underwent a dual time-point [^{18}F]florbetaben (FBB) amyloid MR/PET examination (Fig. 1). The examination revealed cortical Aβ pathology. Further, the early after administration FBB PET images showed a reduced tracer uptake in the bilateral temporal cortex (white arrows), indication neuronal injury in these regions. The structural MR did not reveal any atrophy. Overall, in this patient the MR/PET imaging biomarker-supported diagnosis of MCI due to AD was established.

Relative quantitative parameters

The visual analysis of the PET and MR images is supplemented by relative quantitative parameters. Hippocampal or medial temporal lobe atrophy can be scored by the Scheltens scale [6], whereas white matter lesions can be scored by Fazekas scale [7]. For the late after administration FBB PET data, the established composite SUV ratio can be calculated by averaging the SUV ratios of the frontal, lateral temporal, parietal, occipital, anterior and posterior cingulate cortices, whereby the bilateral cerebellar cortex is used as reference region [8].

Taken together, simultaneous MR/PET imaging in MCI and dementia provides AD biomarker information of both the amyloid pathology and neuronal injury categories, by that supplementing the clinical diagnosis in a fast and convenient manner.

References

1 Albert, Marilyn S.; DeKosky, Steven T.; Dickson, Dennis; Dubois, Bruno; Feldman, Howard H.; Fox, Nick C. et al. (2011): The diagnosis of mild cognitive impairment due to Alzheimer's disease: recommendations from the National Institute on Aging-Alzheimer's Association workgroups on diagnostic guidelines for Alzheimer's disease. In: Alzheimer's & dementia : the journal of the Alzheimer's Association 7 (3), S. 270–279. DOI: 10.1016/j.jalz.2011.03.008.

2 Barthel, Henryk; Gertz, Hermann-Josef; Dresel, Stefan; Peters, Oliver; Bartenstein, Peter; Buerger, Katharina et al. (2011): Cerebral amyloid-β PET with florbetaben (18F) in patients with Alzheimer's disease and healthy controls. a multicentre phase 2 diagnostic study. In: Lancet neurology 10 (5), S. 424–435.

3 Dubois, Bruno; Feldman, Howard H.; Jacova, Claudia; Hampel, Harald; Molinuevo, José Luis; Blennow, Kaj et al. (2014): Advancing research diagnostic criteria for Alzheimer's disease. the IWG-2 criteria. In: The Lancet. Neurology 13 (6), S. 614–629.

4 Fazekas, F.; Chawluk, J. B.; Alavi, A.; Hurtig, H. I.; Zimmerman, R. A. (1987): MR signal abnormalities at 1.5 T in Alzheimer's dementia and normal aging. In: AJR. American journal of roentgenology 149 (2), S. 351–356. DOI: 10.2214/ajr.149.2.351.

5 Garibotto, Valentina; Morbelli, Silvia; Pagani, Marco (2016): Erratum to: Dual-phase amyloid PET: hitting two birds with one stone. In: European journal of nuclear medicine and molecular imaging 43 (9), S. 1747. DOI: 10.1007/s00259-016-3426-1.

6 McKhann, Guy M.; Knopman, David S.; Chertkow, Howard; Hyman, Bradley T.; Jack, Clifford R.; Kawas, Claudia H. et al. (2011): The diagnosis of dementia due to Alzheimer's disease. recommendations from the National Institute on Aging-Alzheimer's Association workgroups on diagnostic guidelines for Alzheimer's disease. In: Alzheimer's & dementia : the journal of the Alzheimer's Association 7 (3), S. 263–269.

7 Scheltens, P.; Leys, D.; Barkhof, F.; Huglo, D.; Weinstein, H. C.; Vermersch, P. et al. (1992): Atrophy of medial temporal lobes on MRI in "probable" Alzheimer's disease and normal ageing: diagnostic value and neuropsychological correlates. In: Journal of neurology, neurosurgery, and psychiatry 55 (10), S. 967–972.

8 Schütz, Lisa; Lobsien, Donald; Fritzsch, Dominik; Tiepolt, Solveig; Werner, Peter; Schroeter, Matthias L. et al. (2016): Feasibility and acceptance of simultaneous amyloid PET/MRI. In: European journal of nuclear medicine and molecular imaging 43 (12), S. 2236–2243. DOI: 10.1007/s00259-016-3462-x.

Contact

Osama Sabri, M.D., Ph.D.
University Professor, Director and Chairman
Department of Nuclear Medicine
University of Leipzig
Liebigstraße 18
04103 Leipzig
Germany
Tel.: +49-341-9718000
Fax: +49-341-9718129
osama.sabri@medizin.uni-leipzig.de

Henryk Barthel, M.D., Ph.D.
Assistant Medical Director
Neuro-PET and PET-MRI
Department of Nuclear Medicine
University of Leipzig
Liebigstraße 18
04103 Leipzig
Germany
Tel.: +49-341-9718082
Fax: +49-341-9718069
henryk.barthel@medizin.uni-leipzig.de

Solveig Tiepolt, M.D.
Assistant Medical Director
Department of Nuclear Medicine
University of Leipzig
Liebigstraße 18
04103 Leipzig
Germany
Tel.: +49-341-9718264
Fax: +49-341-9718129
solveig.tiepolt@medizin.uni-leipzig.de

Application of MR/PET in Pediatric Epilepsy

Michael Kean, FSMRT

Children's MRI and PET Centre, Royal Children's Hospital, Melbourne, Australia

Introduction

There are two papers that are integral to the development of an MR/PET service, Catana: "PET and MR Imaging: The Odd Couple or a Match Made in Heaven" [1] and Gillies: "PET and MRI: Is the Whole Greater than the Sum of Its Parts?" [2].

The success of our MR/PET program is based on a collaborative team approach and the strengths of the individual components work in harmony for the best outcome for the patient.

The Royal Children's hospital is a quaternary referral centre for the treatment of many complex pediatric conditions including congenital heart disease, organ transplantation (heart, liver and small bowel), neuro-oncology and epilepsy surgery. The comprehensive epilepsy program sees 1200 patients each year and account for 12% of all MR referrals and approximately 28% of patients referred for MR/PET.

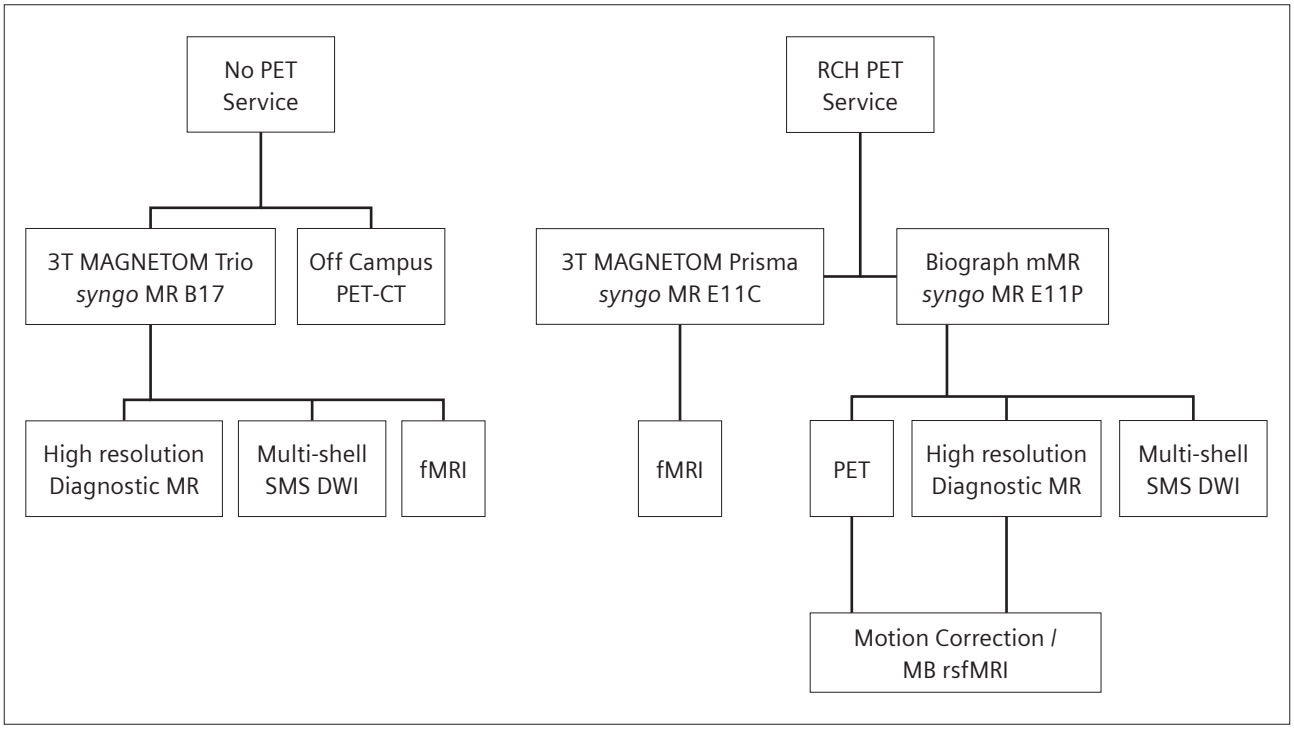

1 Royal Children's Hospital (RCH) MR/PET diagnostic schematic

The Royal Children's Hospital commenced clinical MR/PET imaging in May 2016 and have scanned in excess of 350 pediatric[1] patients with a clinical presentation of epilepsy. The MR/PET is the only PET system at the hospital and prior to its installation PET patients were referred to adult centres for their PET examinations or managed without PET imaging.

The decision to install an MR/PET solution rather than a PET/CT was framed around three key differentials:

- limited space within the medical imaging department to install a PET solution and increase MR capacity
- desire to reduce radiation burden to our patients
- diagnostic sensitivity of CT – lower soft tissue contrast when compared to MR; the functional capabilities of MR (DWI, spectroscopy, perfusion and fingerprinting); and in many clinical areas the higher diagnostic sensitivity of MR.

The introduction of this new imaging modality at our hospital enabled the MR and Nuclear Medicine services to challenge our current standard of care protocols for imaging our epilepsy patients and translate the majority of imaging for our comprehensive epilepsy program to the MR/PET.

Indications

The ongoing structural damage to the brain and socioeconomic consequences of seizures refractory to current pharmacological management is considerable and has been reported to represent up to 30% of patients with partial seizures. In children up to 40% of these cases will exhibit some degree of malformation of cortical development (MCD) either focal or diffuse [3, 4]. PET referrals are predominantly for suspected focal cortical dysplasias (FCD) and to a lesser degree encephalitis and evaluation of pre-operative workup of Tuberous Sclerosis lesions and Sturge Weber. FCD's are sub-grouped into four distinct types Ia, Ib, IIa, IIb based on histology, genetic markers and topographical locations and the improved diagnostic sensitivity of MR/PET has increased our identification of these lesions. The addition of the PET information has further increased our diagnostic specificity of the MR data.

Most of our PET examinations are inter-ictal and the identification of hypo-metabolic anatomical locations will assist in planning surgery. In most clinical presentations the PET and MR are complimentary but in MR negative scans the PET will assist in locating an MR abnormality. In cases of subtle PET hypo-metabolic activity the MR may improve the diagnostic accuracy.

We have done a number of ictal PET studies when further diagnostic information is required in complex or post operative cases where PET and MR demonstrate conflicting results.

Review papers [5–9] have identified a number of key factors that increase the percentage of 'MR negative' studies, these include – but are not limited to – experience of reader, not performed with appropriate field strength, variation in sequences, poor slice orientation, poor clinical information, and no quantitative analysis.

The ability of MR and PET to identify abnormal dysplastic tissue is also related to the degree of histopathological derangement of the tissue.

Imaging

In researching the literature prior to commencing our clinical service it was clear that many sites failed to extract the full potential of the MR component of the MR/PET mainly due to lower density head coils placing a higher emphasis on the PET acquisition so our objectives were:

- enhance the diagnostic yield of MR and PET focusing on the strengths of both modalities,
- motion correction of MR and PET data,
- reduction in radiation burden, and
- patient focused care combining multiple appointments into a single scanning session and reducing the need for multiple anesthetics.

The goal of any epilepsy imaging service is that it must be multidisciplinary, identify physiological and anatomic biomarkers of the epileptogenic zone, be undertaken at high field strengths using standardized PET and MR imaging protocols, qualitative and quantitative analysis of PET and MR data, informed reporting where all diagnostic and clinical data is available to the reporting specialist [10–14].

Maintaining the sensitivity and specificity of our current MR protocols when transferring these patients to the hybrid MR/PET was crucial to the success of our epilepsy program. The sensitivity and specificity of any epilepsy protocol is dramatically affected by the MR system field strength, availability of high density array coils, access to the latest MR sequences and an understanding of methods to extract the highest resolution scans from the system.

Our MR epilepsy imaging protocols were developed on a 3T MAGNETOM Trio running *syngo* MR B17 software and 3T MAGNETOM Prisma^{fit} (*syngo* MR E11 software), using a product 32-channel head coil. These protocols included T2 transverse / coronal TSE 2.5 x 0.3 x 0.3 mm, T2 sagittal 1.5 x 0.3 x 0.3 mm, 0.9 mm 3D FS FLAIR, 0.8 mm

[1] *MR scanning has not been established as safe for imaging fetuses and infants less than two years of age. The responsible physician must evaluate the benefits of the MR examination compared to those of other imaging procedures. Note: This disclaimer does not represent the opinion of the author.*

T1 MPRAGE and multi-shell SMS DWI 2.3 x 2.3 x 2.3 mm (*b*-values = 1000, 2000, 3000 s/mm^2; Tract analysis using MRTrix[1] and advanced metrics such as neurite orientation dispersion and density imaging (NODDI) and SWI/QSM. Transferring protocols between different MR systems and software versions can lead to potential issues with image quality especially signal to noise variations. The key to maintaining image quality and diagnostic epilepsy imaging of a high standard is a thorough understanding of the internals of your system (coil platform, RF-technology and receive chain, sequences).

The complexities of obtaining, adapting, implementing, and maintaining both PET and MR imaging protocols [15, 16] with a higher density head MR are not trivial. We developed the coil correction maps for the 32-channel head coil[2] in conjunction with our local Siemens Healthineers scientists.

Prior to implementing these scans clinically comparative studies were undertaken to compare the diagnostic accuracy of PET and MR including the attenuation correction and diagnostic sequences obtained with the standard MR/PET coil and the 32-channel version.

An example of our current synergistic protocol is shown in Figure 2. One of key objectives was to reduce radiation dose and this has been accomplished with an administered dose reduction of 50% compared to current PET/CT dosing. Our current PET protocol is an administered dose 2 MBq/kg of ^{18}FDG with the PET acquired for 20 mins in list mode (HD PET, 3 iterations, 21 subsets 2.5 mm FWHM and 344 resolution) with or without motion correction.

The question of attenuation correction in brain imaging is a complex one and although the consensus from the 6th Tubingen workshop [17] was "the case of MR-based attenuation correction is closed" we feel that it may not necessarily be the case in pediatrics given the diversity of head sizes, structure of the cranial vault as reflected by their age, and variation in T1/T2 relaxation times of the brain based on the patients age. We are presented with many options for attenuation correction from emission based protocols, segmentation techniques using a variety of MR pulse sequence (Dixon, UTE[2], ZTE[2]), atlas/template based approaches or more recently CNN based approaches [18-24]. Currently, for consistency of results our method of choice is a segmentation combined atlas approach using standard 3D Dixon T1 but we are currently exploring CNN based approaches.

Patient motion is an integral part of pediatric imaging and the capability of obtaining motion free images for our PET and MR acquisitions is paramount. Outside of sedating your patient there are a number of commercially available solutions to correct for motion in the PET and MR data. The simplest approach is training your patient via mock MRI programs, interactive online modules or restraints within the head coil. Our approach reflects the age and clinical presentation of the patient and options range from anesthesia, minimal oral sedation, mock MRI with our Child Life Specialists, good audio-visual distraction during scanning and a team approach to working with the patients and their families to enable a positive experience. A robust method of motion correcting PET and MR data is driven by the MR acquisition [25–27]. This approach is robust and provides consistency of results without the additional cost of optical tracking cameras. In our patient cohort we use rigid motion correction using the BrainCOMPASS option provided by Siemens Healthineers in approximately 20% of our patients. Our first implementation of BrainCOMPASS used the standard BOLD acquisition from the sequence library. In recent times we have a number of sequence options that can be incorporated into the motion correction algorithm based on our evaluation of the patient. Our first deviation from the standard was to implement SMS BOLD sequence[2] into the protocol reducing the TR to increase our temporal resolution potentially improving the resultant motion corrected image and an added benefit gain some resting state data for connectomics. In patients where we feel there may be minimal movement we use the motion data obtained from an epi NavMPRAGE[2] to retrospectively correct the PET data. Currently approximately 26% of our patients are scanned using the epi Navigator 3D MPRAGE sequence.

Last but definitely not the least important is to improve the diagnostic quality of the PET data and there are many groups evaluating different approaches to driving the increased resolution of the PET data. PET reconstruction driven by the MR data is an exciting new era in PET reconstruction techniques combining AI and CNN approaches [29–32].

[1]The information shown herein refers to products of 3rd party manufacturers and thus are in their regulatory responsibility. Please contact the 3rd party manufacturer for further information.

[2]Work in progress: the application / the coil is currently under development and is not for sale in the U.S. and in other countries. Its future availability cannot be ensured.

MRAC	PET – 20 mins (HD PET, 3 iterations / 2.5 mm FHWHM PSF 344)					
	3D T1	T2 tra	T2 cor	3D T2 FLAIR	T2 sag	SMS DWI (3 shells)

2 MR/PET acquisition workflow

Conclusion

The installation of a synergistic MR/PET solution within our imaging department has significantly improved the quality of care to our epilepsy patients. The clinical acceptance within the hospital has been a significant factor in integrating our comprehensive epilepsy program to the MR/PET. The introduction of a higher density coil in the initial stages of our service has dramatically improved the MR images. Continual advances in attenuation correction and motion correction have further increased our diagnostic sensitivity. The new imaging modality, as we refer to it, required re-evaluation of how we deliver our care to our patients but it has been well accepted by clinicians, patients, and families.

We are very enthusiastic about where this technology is heading with further technological advancements in pulse sequences, image reconstruction methodology including AI, and motion correction.

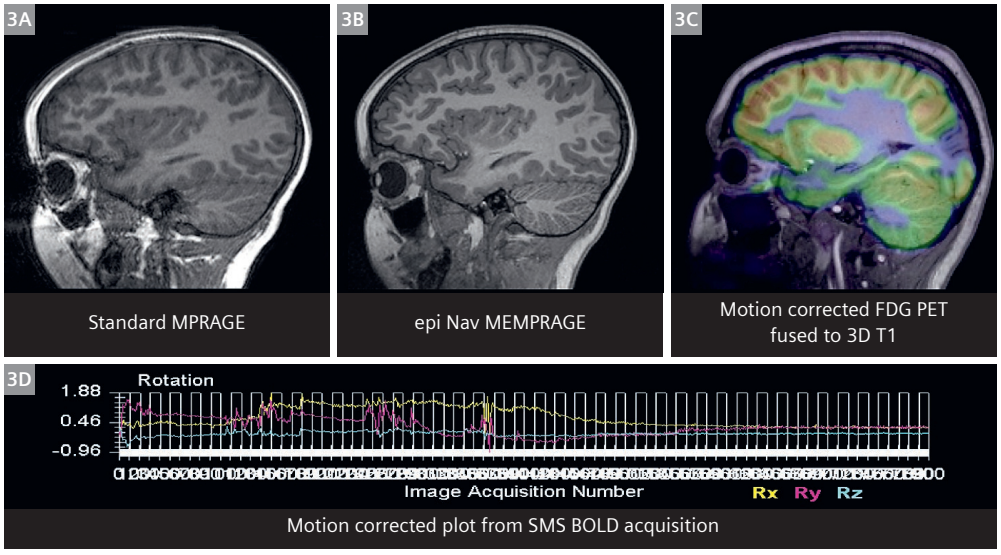

3 **(3A)** Standard 3D T1 MPRAGE demonstrating patient movement. **(3**B) Navigator motion corrected Multi-echo MPRAGE (MEMPRAGE). **(3C)** Motion corrected FDG PET fused to 3D MPRAGE. **(3D)** Motion plot from BrainCOMPASS SMS BOLD acquisition.

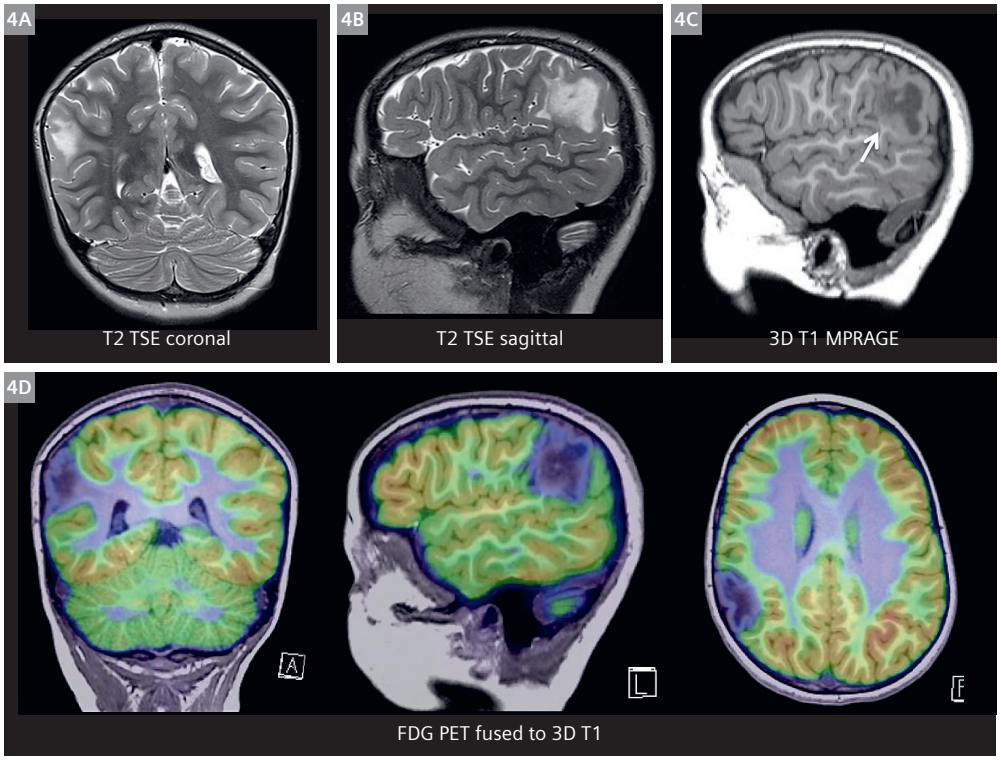

4 Patient referred for MR/PET with suspected FCD on outside 1.5T non-epilepsy protocol scan.

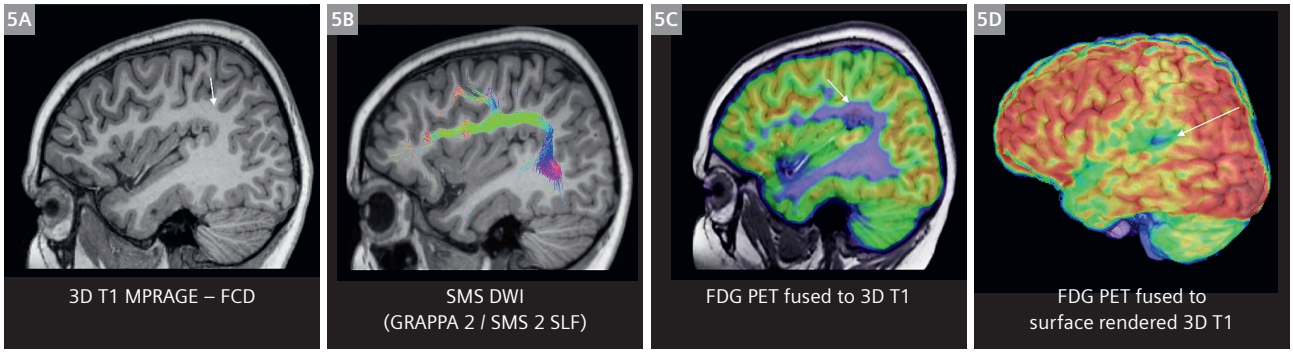

5 Patient presented with refractory partial seizures during her seizures she had absences, aphasia and falls. Imaging: **(5A)** 3D T1 MPRAGE demonstrating FCD. **(5B)** Tract representation of Superior Longitudinal Fasiculus (SLF). **(5C)** FDG PET demonstrates hypo-metabolic region of MR abnormality. **(5D)** Surface rendered 3D T1 with PET overlay demonstrating the surgical window.

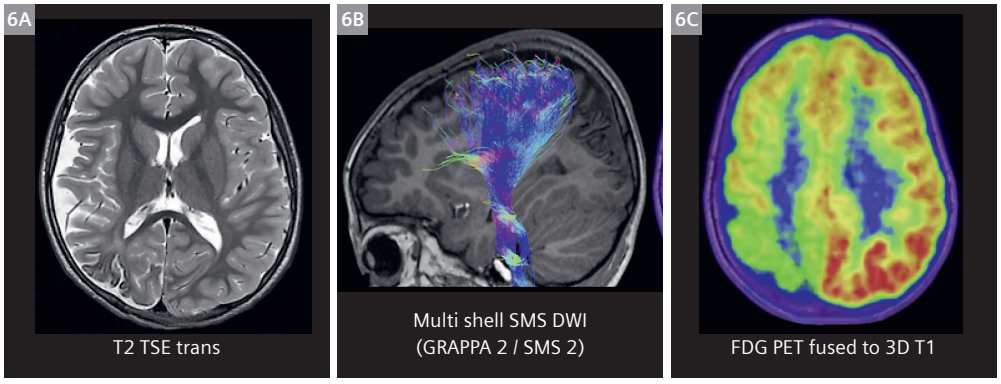

6 Patient with Sturge Weber without hemiplegia. **(6A)** T2 transverse image demonstrating atrophy associated with Sturge Weber. **(6B)** Pre-operative SMS DWI with cortico-spinal tracts. Patient underwent a TPO disconnection preserving motor function.

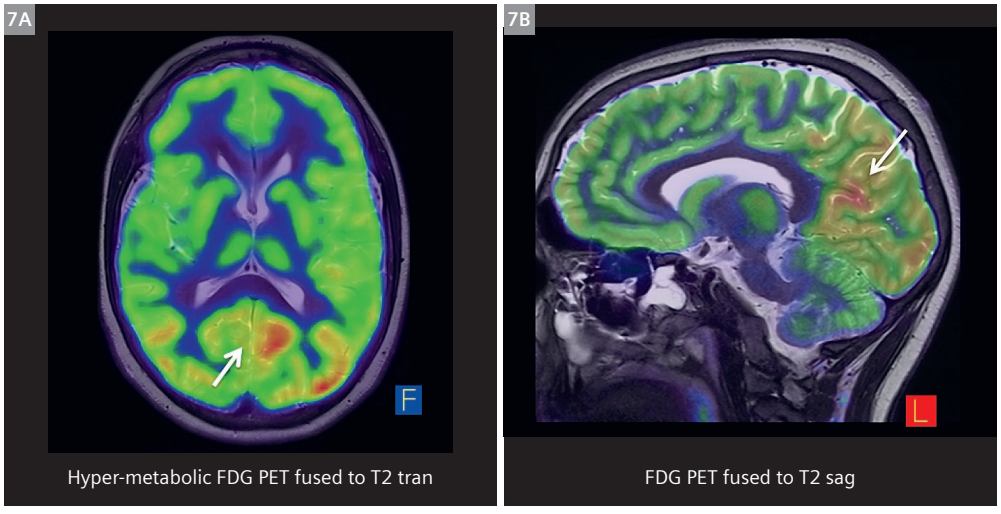

7 Patient presented with epileptic spikes demonstrated on a sleep EEG recording with normal awake EEG. MR PET acquired after 60 mins quiet resting demonstrates hyper-metabolic region.

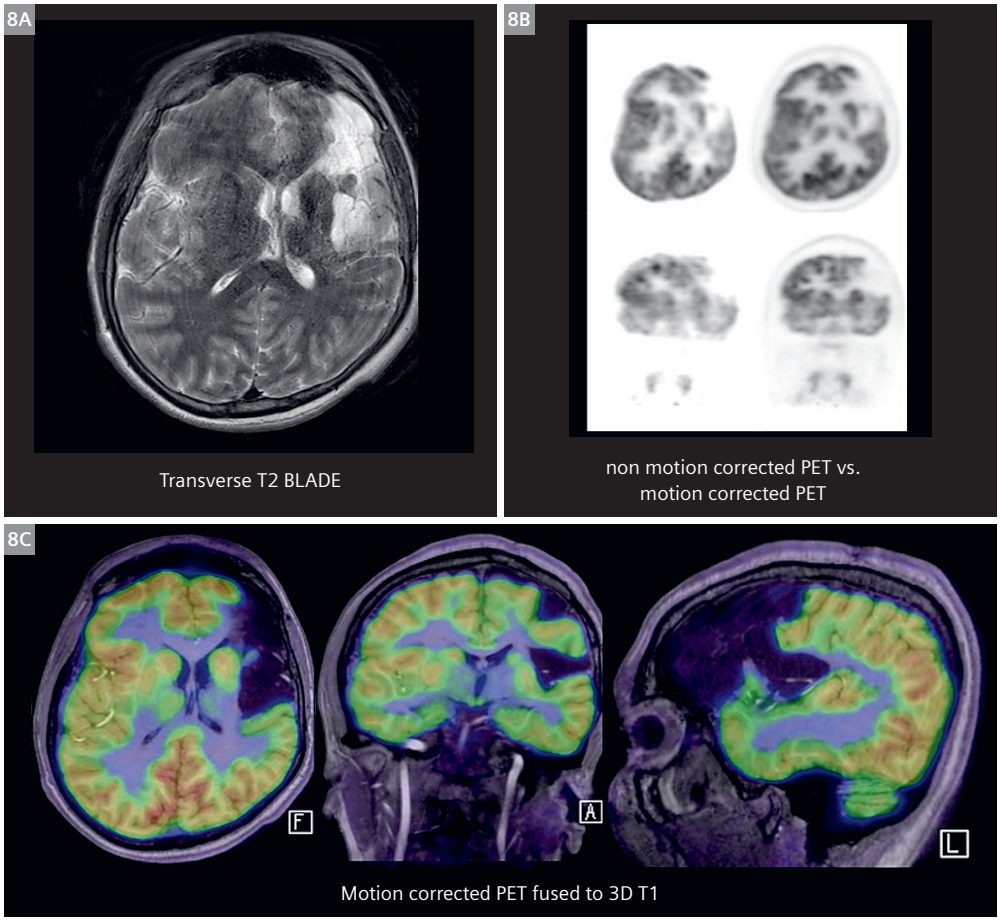

8 Patient presented with ongoing seizures two years post resection of cortical dysplasia overseas. Patient was borderline assessment for a wake MR/PET and was scanned using BrainCOMPASS. T2 BLADE is severely degraded by patient movement but using the MR derived motion data a diagnostic PET was obtained.

References

1 Catana, C., Guimaraes, A.R. & Rosen, B.R., 2013. PET and MR Imaging: The Odd Couple or a Match Made in Heaven? Journal of Nuclear Medicine, 54(5), pp.815–824.

2 Gillies, R.J. & Beyer, T., 2016. PET and MRI: Is the Whole Greater than the Sum of Its Parts? Cancer Research, 76(21), pp.6163–6166.

3 Barkovich, A.J., Dobyns, W.B. & Guerrini, R., 2015. Malformations of Cortical Development and Epilepsy. Cold Spring Harbor Perspectives in Medicine, 5(5), pp.a022392–a022392.

4 Desikan, R.S. & Barkovich, A.J., 2016. Malformations of cortical development. Annals of Neurology, 80(6), pp.797–810.

5 Bernasconi, N. & Bernasconi, A., 2014. Epilepsy: Imaging the epileptic brain – time for new standards. Nature Publishing Group, 10(3), pp.133–134.

6 Bernasconi, A. et al., 2011. Advances in MRI for "cryptogenic" epilepsies. Nature Publishing Group, 7(2), pp.99–108.

7 Wellmer, J. et al., 2013. Proposal for a magnetic resonance imaging protocol for the detection of epileptogenic lesions at early outpatient stages. Epilepsia, 54(11), pp.1977–1987.

8 Winston, G.P. et al., 2013. The value of repeat neuroimaging for epilepsy at a tertiary referral centre: 16 years of experience. Epilepsy Research, 105(3), pp.349–355.

9 Zijlmans, M. et al., 2009. 3T versus 1.5T phased-array MRI in the presurgical work-up of patients with partial epilepsy of uncertain focus. Journal of magnetic resonance imaging: JMRI, 30(2), pp.256–262.

10 Pardoe, H. & Kuzniecky, R., 2014. Advanced Imaging Techniques in the Diagnosis of Nonlesional Epilepsy: MRI, MRS, PET, and SPECT. Epilepsy currents, 14(3), pp.121–124.

11 Pestana Knight, E.M., Gonzalez-Martinez, J. & Gupta, A., 2015. Pre-operative evaluation in pediatric patients with cortical dysplasia. Child's nervous system : 31(12), pp.2225–2233.

12 Kim, S. et al., 2009. PET imaging in pediatric neuroradiology: current and future applications. Pediatric Radiology, 40(1), pp.82–96.

13 Klooster, M.A.V. et al., 2014. Can we increase the yield of FDG-PET in the preoperative work-up for epilepsy surgery? Epilepsy Research, 108(6), pp.1095–1105.

14 Chen, K.T., Salcedo, S., Gong, K., Chonde, D.B., Izquierdo-Garcia, D., Drzezga, A., Rosen, B., Qi, J., Dickerson, B.C. and Catana, C., 2019. An efficient approach to perform MR-assisted PET data optimization in simultaneous PET/MR neuroimaging studies. Journal of Nuclear Medicine, 60(2), pp.272-278.

15 Oldan, J.D. et al., 2018. Subsequent experience in hybrid PET-MRI for evaluation of refractory focal onset epilepsy. Seizure: European Journal of Epilepsy, 61, pp.128–134.

16 Desarnaud, S. et al., 2018. 18F-FDG PET in drug-resistant epilepsy due to focal cortical dysplasia type 2: additional value of electroclinical data and coregistration with MRI. pp.1–12.

17 Mehranian, A., Zaidi, H., & Reader, A. J. (2017). MR-guided joint reconstruction of activity and attenuation in brain PET-MR. NeuroImage, 162, 276–288.

18 Bailey, D.L. et al., 2018. Combined PET/MRI: Global Warming – Summary Report of the 6th International Workshop on PET/MRI, March 27–29, 2017, Tübingen, Germany. pp.1–17.
19 Catana, C., Quick, H. and Zaidi, H., 2018. Current commercial techniques for MRI-guided attenuation correction are insufficient and will limit the wider acceptance of PET/MRI technology in the clinic. Medical physics, 45(9), pp.4007-4010.
20 Mehranian, A., Arabi, H. and Zaidi, H., 2016. Vision 20/20: Magnetic resonance imaging-guided attenuation correction in PET/MRI: Challenges, solutions, and opportunities. Medical Physics, 43(3), pp.1130–1155.
21 Izquierdo-Garcia, D. et al., 2018. Intrascanner Reproducibility of an SPM-based Head MR-based Attenuation Correction Method. Intrascanner Reproducibility of an SPM-based Head MR-based Attenuation Correction Method. IEEE Transactions on Radiation and Plasma Medical Sciences.
22 Ladefoged, C.N. et al., 2017. A multi-centre evaluation of eleven clinically feasible brain PET/MRI attenuation correction techniques using a large cohort of patients. NeuroImage, 147(C), pp.346–359.
23 Koesters, T. et al., 2016. Dixon Sequence with Superimposed Model-Based Bone Compartment Provides Highly Accurate PET/MR Attenuation Correction of the Brain. Journal of Nuclear Medicine, 57(6), pp.918–924.
24 Jang, H. et al., 2018. Technical Note: Deep learning based MRAC using rapid ultrashort echo time imaging. Medical Physics, 45(8), pp.3697–3704.
25 Izquierdo-Garcia, D., Hansen, A.E., Förster, S., Benoit, D., Schachoff, S., Fürst, S., Chen, K.T., Chonde, D.B. and Catana, C., 2014. An SPM8-based approach for attenuation correction combining segmentation and nonrigid template formation: application to simultaneous PET/MR brain imaging. Journal of Nuclear Medicine, 55(11), pp.1825-1830.
26 Catana, C., Benner, T., van der Kouwe, A., Byars, L., Hamm, M., Chonde, D. B. and Sorensen, A. G. (2011). MRI-assisted PET motion correction for neurologic studies in an integrated MR-PET scanner. Journal of Nuclear Medicine, 52,(1) 154–161.
27 Tisdall, M.D., Hess, A.T., Reuter, M., Meintjes, E.M., Fischl, B. and van der Kouwe, A.J., 2012. Volumetric navigators for prospective motion correction and selective reacquisition in neuroanatomical MRI. Magnetic resonance in medicine, 68(2), pp.389-399.
28 Ullisch, M.G. et al., 2012. MR-Based PET Motion Correction Procedure for Simultaneous MR-PET Neuroimaging of Human Brain C.-T. Chen, ed. PLoS ONE, 7(11), pp.e48149–13.
29 Liu, F., Jang, H., Kijowski, R., Bradshaw, T. and McMillan, A.B., 2017. Deep learning MR imaging–based attenuation correction for PET/MR imaging. Radiology, 286(2), pp.676-684.
30 Chen, K.T., Salcedo, S., Gong, K., Chonde, D.B., Izquierdo-Garcia, D., Drzezga, A., Rosen, B., Qi, J., Dickerson, B.C. and Catana, C., 2019. An efficient approach to perform MR-assisted PET data optimization in simultaneous PET/MR neuroimaging studies. Journal of Nuclear Medicine, 60(2), pp.272-278.
31 Spuhler, K.D., Gardus, J., Gao, Y., DeLorenzo, C., Parsey, R. and Huang, C., 2018. Synthesis of patient-specific transmission image for PET attenuation correction for PET/MR imaging of the brain using a convolutional neural network. Journal of Nuclear Medicine, pp.jnumed-118.
32 Schramm, G., Holler, M., Rezaei, A., Vunckx, K., Knoll, F., Bredies, K., Boada, F. and Nuyts, J., 2018. Evaluation of parallel level sets and Bowsher's method as segmentation-free anatomical priors for time-of-flight PET reconstruction. IEEE transactions on medical imaging, 37(2), pp.590-603
33 Mehranian, A., Belzunce, M., Prieto, C., Hammers, A., & Reader, A. (2018). Synergistic PET and SENSE MR image reconstruction using joint sparisity regularization. IEEE Transactions on Medical Imaging. 37, 20–34.

Contact

Michael Kean, FSMRT
Chief MR Technologist
Children's MRI and PET Centre
Department of Medical Imaging
Honorary Fellow, Developmental Imaging,
Murdoch Children's Research Institute
Honorary Senior Research Fellow,
Department of Paediatrics,
The University of Melbourne
Royal Children's Hospital,
Flemington Road
Parkville
Australia
Tel.: +61 411681198
Michael.Kean@rch.org.au

HIGHLIGHTS OF PRESCRIBING INFORMATION

These highlights do not include all the information needed to use Fludeoxyglucose F 18 Injection safely and effectively. See full prescribing information for Fludeoxyglucose F 18 Injection. Fludeoxyglucose F 18 Injection, USP For intravenous use Initial U.S. Approval: 2005

RECENT MAJOR CHANGES

Warnings and Precautions (5.1, 5.2)	7/2010
Adverse Reactions (6)	7/2010

INDICATIONS AND USAGE

Fludeoxyglucose F18 Injection is indicated for positron emission tomography (PET) imaging in the following settings:

- Oncology: For assessment of abnormal glucose metabolism to assist in the evaluation of malignancy in patients with known or suspected abnormalities found by other testing modalities, or in patients with an existing diagnosis of cancer.
- Cardiology: For the identification of left ventricular myocardium with residual glucose metabolism and reversible loss of systolic function in patients with coronary artery disease and left ventricular dysfunction, when used together with myocardial perfusion imaging.
- Neurology: For the identification of regions of abnormal glucose metabolism associated with foci of epileptic seizures (1).

DOSAGE AND ADMINISTRATION

Fludeoxyglucose F 18 Injection emits radiation. Use procedures to minimize radiation exposure. Screen for blood glucose abnormalities.

- In the oncology and neurology settings, instruct patients to fast for 4 to 6 hours prior to the drug's injection. Consider medical therapy and laboratory testing to assure at least two days of normoglycemia prior to the drug's administration (5.2).
- In the cardiology setting, administration of glucose-containing food or liquids (e.g., 50 to 75 grams) prior to the drug's injection facilitates localization of cardiac ischemia (2.3).

Aseptically withdraw Fludeoxyglucose F 18 Injection from its container and administer by intravenous injection (2).

The recommended dose:

- for adults is 5 to 10 mCi (185 to 370 MBq), in all indicated clinical settings (2.1).
- for pediatric patients is 2.6 mCi in the neurology setting (2.2).

Initiate imaging within 40 minutes following drug injection; acquire static emission images 30 to 100 minutes from time of injection (2).

DOSAGE FORMS AND STRENGTHS

Multi-dose 30mL and 50mL glass vial containing 0.74 to 7.40 GBq/mL (20 to 200 mCi/mL) Fludeoxyglucose F 18 Injection and 4.5mg of sodium chloride with 0.1 to 0.5% w/w ethanol as a stabilizer (approximately 15 to 50 mL volume) for intravenous administration (3).

CONTRAINDICATIONS

None

WARNINGS AND PRECAUTIONS

- Radiation risks: use smallest dose necessary for imaging (5.1).
- Blood glucose adnormalities: may cause suboptimal imaging (5.2).

ADVERSE REACTIONS

Hypersensitivity reactions have occurred; have emergency resuscitation equipment and personnel immediately available (6).

To report SUSPECTED ADVERSE REACTIONS, contact PETNET Solutions, Inc. at 877-473-8638 or FDA at 1-800-FDA-1088 or www.fda.gov/medwatch.

USE IN SPECIFIC POPULATIONS

Pregnancy Category C: No human or animal data. Consider alternative diagnostics; use only if clearly needed (8.1).

- Nursing mothers: Use alternatives to breast feeding (e.g., stored breast milk or infant formula) for at least 10 half-lives of radioactive decay, if Fludeoxyglucose F 18 Injection is administered to a woman who is breast-feeding (8.3).
- Pediatric Use: Safety and effectiveness in pediatric patients have not been established in the oncology and cardiology settings (8.4).

See 17 for PATIENT COUNSELING INFORMATION

Revised: 1/2011

FULL PRESCRIBING INFORMATION: CONTENTS*

*Sections or subsections omitted from the full prescribing information are not listed.

FULL PRESCRIBING INFORMATION

1 INDICATIONS AND USAGE

Fludeoxyglucose F 18 Injection is indicated for positron emission tomography (PET) imaging in the following settings:

1.1 Oncology

For assessment of abnormal glucose metabolism to assist in the evaluation of malignancy in patients with known or suspected abnormalities found by other testing modalities, or in patients with an existing diagnosis of cancer.

1.2 Cardiology

For the identification of left ventricular myocardium with residual glucose metabolism and reversible loss of systolic function in patients with coronary artery disease and left ventricular dysfunction, when used together with myocardial perfusion imaging.

1.3 Neurology

For the identification of regions of abnormal glucose metabolism associated with foci of epileptic seizures.

2 DOSAGE AND ADMINISTRATION

Fludeoxyglucose F 18 Injection emits radiation. Use procedures to minimize radiation exposure. Calculate the final dose from the end of synthesis (EOS) time using proper radioactive decay factors. Assay the final dose in a properly calibrated dose calibrator before administration to the patient [see Description (11.2)].

2.1 Recommended Dose for Adults

Within the oncology, cardiology and neurology settings, the recommended dose for adults is 5 to 10 mCi (185 to 370 MBq) as an intravenous injection.

2.2 Recommended Dose for Pediatric Patients

Within the neurology setting, the recommended dose for pediatric patients is 2.6 mCi, as an intravenous injection. The optimal dose adjustment on the basis of body size or weight has not been determined [see Use in Special Populations (8.4)].

2.3 Patient Preparation

- To minimize the radiation absorbed dose to the bladder, encourage adequate hydration. Encourage the patient to drink water or other fluids (as tolerated) in the 4 hours before their PET study.
- Encourage the patient to void as soon as the imaging study is completed and as often as possible thereafter for at least one hour.
- Screen patients for clinically significant blood glucose abnormalities by obtaining a history and/or laboratory tests [see Warnings and Precautions (5.2)]. Prior to Fludeoxyglucose F 18 PET imaging in the oncology and neurology settings, instruct patient to fast for 4 to 6 hours prior to the drug's injection.
- In the cardiology setting, administration of glucose-containing food or liquids (e.g., 50 to 75 grams) prior to Fludeoxyglucose F18 Injection facilitates localization of cardiac ischemia

2.4 Radiation Dosimetry

The estimated human absorbed radiation doses (rem/mCi) to a newborn (3.4 kg), 1-year-old (9.8 kg), 5-year-old (19 kg), 10-year-old (32 kg), 15-year-old (57 kg), and adult (70 kg) from intravenous administration of Fludeoxyglucose F 18 Injection are shown in Table 1. These estimates were calculated based on human[2] data and using the data published by the International Commission on Radiological Protection[4] for Fludeoxyglucose ^{18}F. The dosimetry data show that there are slight variations in absorbed radiation dose for various organs in each of the age groups. These dissimilarities in absorbed radiation dose are due to developmental age variations (e.g., organ size, location, and overall metabolic rate for each age group). The identified critical organs (in descending order) across all age groups evaluated are the urinary bladder, heart, pancreas, spleen, and lungs.

Table 1. Estimated Absorbed Radiation Doses (rem/mCi) After Intravenous Administration of Fludeoxyglucose F-18 Injection[a]

Organ	Newborn (3.4 kg)	1-year-old (9.8 kg)	5-year-old (19 kg)	10-year-old (32 kg)	15-year-old (57 kg)	Adult (70 kg)
Bladder wall[b]	4.3	1.7	0.93	0.60	0.40	0.32
Heart wall	2.4	1.2	0.70	0.44	0.29	0.22
Pancreas	2.2	0.68	0.33	0.25	0.13	0.096
Spleen	2.2	0.84	0.46	0.29	0.19	0.14
Lungs	0.96	0.38	0.20	0.13	0.092	0.064
Kidneys	0.81	0.34	0.19	0.13	0.089	0.074
Ovaries	0.80	0.8	0.19	0.11	0.058	0.053
Uterus	0.79	0.35	0.19	0.12	0.076	0.062
LLI wall *	0.69	0.28	0.15	0.097	0.060	0.051
Liver	0.69	0.31	0.17	0.11	0.076	0.058
Gallbladder wall	0.69	0.26	0.14	0.093	0.059	0.049
Small intestine	0.68	0.29	0.15	0.096	0.060	0.047
ULI wall **	0.67	0.27	0.15	0.090	0.057	0.046
Stomach wall	0.65	0.27	0.14	0.089	0.057	0.047
Adrenals	0.65	0.28	0.15	0.095	0.061	0.048
Testes	0.64	0.27	0.14	0.085	0.052	0.041
Red marrow	0.62	0.26	0.14	0.089	0.057	0.047
Thymus	0.61	0.26	0.14	0.086	0.056	0.044
Thyroid	0.61	0.26	0.13	0.080	0.049	0.039
Muscle	0.58	0.25	0.13	0.078	0.049	0.039
Bone surface	0.57	0.24	0.12	0.079	0.052	0.041
Breast	0.54	0.22	0.11	0.068	0.043	0.034
Skin	0.49	0.20	0.10	0.060	0.037	0.030
Brain	0.29	0.13	0.09	0.078	0.072	0.070
Other tissues	0.59	0.25	0.13	0.083	0.052	0.042

[a] MIRDOSE 2 software was used to calculate the radiation absorbed dose. Assumptions on the biodistribution based on data from Gallagher et al.1 and Jones et al.[2]

[b] The dynamic bladder model with a uniform voiding frequency of 1.5 hours was used.

*LLI = lower large intestine; **ULI = upper large intestine

2.5 Radiation Safety – Drug Handling

- Use waterproof gloves, effective radiation shielding, and appropriate safety measures when handling Fludeoxyglucose F 18 Injection to avoid unnecessary radiation exposure to the patient, occupational workers, clinical personnel and other persons.
- Radiopharmaceuticals should be used by or under the control of physicians who are qualified by specific training and experience in the safe use and handling of radionuclides, and whose experience and training have been approved by the appropriate governmental agency authorized to license the use of radionuclides.
- Calculate the final dose from the end of synthesis (EOS) time using proper radioactive decay factors. Assay the final dose in a properly calibrated dose calibrator before administration to the patient [see Description (11.2)].
- The dose of Fludeoxyglucose F 18 used in a given patient should be minimized consistent with the objectives of the procedure, and the nature of the radiation detection devices employed.

2.6 Drug Preparation and Administration

- Calculate the necessary volume to administer based on calibration time and dose.
- Aseptically withdraw Fludeoxyglucose F 18 Injection from its container.
- Inspect Fludeoxyglucose F 18 Injection visually for particulate matter and discoloration before administration, whenever solution and container permit.
- Do not administer the drug if it contains particulate matter or discoloration; dispose of these unacceptable or unused preparations in a safe manner, in compliance with applicable regulations. Use Fludeoxyglucose F 18 Injection within 12 hours from the EOS.

2.7 Imaging Guidelines

- Initiate imaging within 40 minutes following Fludeoxyglucose F 18 Injection administration.
- Acquire static emission images 30 to 100 minutes from the time of injection.

3 DOSAGE FORMS AND STRENGTHS

Multiple-dose 30 mL and 50 mL glass vial containing 0.74 to 7.40 GBq/mL (20 to 200 mCi/mL) of Fludeoxyglucose F 18 Injection and 4.5 mg of sodium chloride with 0.1 to 0.5% w/w ethanol as a stabilizer (approximately 15 to 50 mL volume) for intravenous administration.

4 CONTRAINDICATIONS

None

5 WARNINGS AND PRECAUTIONS

5.1 Radiation Risks

Radiation-emitting products, including Fludeoxyglucose F 18 Injection, may increase the risk for cancer, especially in pediatric patients. Use the smallest dose necessary for imaging and ensure safe handling to protect the patient and health care worker [see Dosage and Administration (2.5)].

5.2 Blood Glucose Abnormalities

In the oncology and neurology setting, suboptimal imaging may occur in patients with inadequately regulated blood glucose levels. In these patients, consider medical therapy and laboratory testing to assure at least two days of normoglycemia prior to Fludeoxyglucose F 18 Injection administration.

6 ADVERSE REACTIONS

Hypersensitivity reactions with pruritus, edema and rash have been reported in the post-marketing setting. Have emergency resuscitation equipment and personnel immediately available.

7 DRUG INTERACTIONS

The possibility of interactions of Fludeoxyglucose F 18 Injection with other drugs taken by patients undergoing PET imaging has not been studied.

8 USE IN SPECIFIC POPULATIONS

8.1 Pregnancy

Pregnancy Category C

Animal reproduction studies have not been conducted with Fludeoxyglucose F 18 Injection. It is also not known whether Fludeoxyglucose F 18 Injection can cause fetal harm when administered to a pregnant woman or can affect reproduction capacity. Consider alternative diagnostic tests in a pregnant woman; administer Fludeoxyglucose F 18 Injection only if clearly needed.

8.3 Nursing Mothers

It is not known whether Fludeoxyglucose F 18 Injection is excreted in human milk. Consider alternative diagnostic tests in women who are breast-feeding. Use alternatives to breast feeding (e.g., stored breast milk or infant formula) for at least 10 half-lives of radioactive decay, if Fludeoxyglucose F 18 Injection is administered to a woman who is breast-feeding.

8.4 Pediatric Use

The safety and effectiveness of Fludeoxyglucose F 18 Injection in pediatric patients with epilepsy is established on the basis of studies in adult and pediatric patients. In pediatric patients with epilepsy, the recommended dose is 2.6 mCi. The optimal dose adjustment on the basis of body size or weight has not been determined. In the oncology or cardiology settings, the safety and effectiveness of Fludeoxyglucose F 18 Injection have not been established in pediatric patients.

11 DESCRIPTION

11.1 Chemical Characteristics

Fludeoxyglucose F 18 Injection is a positron emitting radiopharmaceutical that is used for diagnostic purposes in conjunction with positron emission tomography (PET) imaging. The active ingredient 2-deoxy-2-[^{18}F]fluoro-D-glucose has the molecular formula of $C_6H_{11}{}^{18}FO_5$ with a molecular weight of 181.26, and has the following chemical structure:

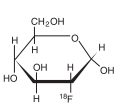

Fludeoxyglucose F 18 Injection is provided as a ready to use sterile, pyrogen free, clear, colorless solution. Each mL contains between 0.740 to 7.40GBq (20.0 to 200 mCi) of 2-deoxy-2-[^{18}F]fluoro-D-glucose at the EOS, 4.5 mg of sodium chloride and 0.1 to 0.5% w/w ethanol as a stabilizer. The pH of the solution is between 4.5 and 7.5. The solution is packaged in a multiple-dose glass vial and does not contain any preservative.

11.2 Physical Characteristics

Fluorine F 18 decays by emitting positron to Oxygen O 16 (stable) and has a physical half-life of 109.7 minutes. The principal photons useful for imaging are the dual 511 keV gamma photons, that are produced and emitted simultaneously in opposite direction when the positron interacts with an electron (Table 2).

Table 2. Pricipal Radiation Emission Data for Fluorine F18		
Radiation/Emission	% Per Disintegration	Mean Energy
Positron (b+)	96.73	249.8 keV
Gamma (±)*	193.46	511.0 keV

*Produced by positron annihilation

From: Kocher, D.C. Radioactive Decay Tables DOE/TIC-I 1026, 89 (1981)

The specific gamma ray constant (point source air kerma coefficient) for fluorine F 18 is 5.7 R/hr/mCi (1.35 x 10-6 Gy/hr/kBq) at 1 cm. The half-value layer (HVL) for the 511 keV photons is 4 mm lead (Pb). The range of attenuation coefficients for this radionuclide as a function of lead shield thickness is shown in Table 3. For example, the interposition of an 8 mm thickness of Pb, with a coefficient of attenuation of 0.25, will decrease the external radiation by 75%.

Table 3. Radiation Attenuation of 511 keV Photons by lead (Pb) shielding	
Shield thickness (Pb) mm	Coefficient of attenuation
0	0.00
4	0.50
8	0.25
13	0.10
26	0.01
39	0.001
52	0.0001

For use in correcting for physical decay of this radionuclide, the fractions remaining at selected intervals after calibration are shown in Table 4.

Table 4. Physical Decay Chart for Fluorine F18	
Minutes	Fraction Remaining
0*	1.000
15	0.909
30	0.826
60	0.683
110	0.500
220	0.250

*calibration time

12 CLINICAL PHARMACOLOGY

12.1 Mechanism of Action

Fludeoxyglucose F 18 is a glucose analog that concentrates in cells that rely upon glucose as an energy source, or in cells whose dependence on glucose increases under pathophysiological conditions. Fludeoxyglucose F 18 is transported through the cell membrane by facilitative glucose transporter proteins and is phosphorylated within the cell to [^{18}F] FDG-6-phosphate by the enzyme hexokinase. Once phosphorylated it cannot exit until it is dephosphorylated by glucose-6-phosphatase. Therefore, within a given tissue or pathophysiological process, the retention and clearance of Fludeoxyglucose F 18 reflect a balance involving glucose transporter, hexokinase and glucose-6-phosphatase activities. When allowance is made for the kinetic differences between glucose and Fludeoxyglucose F 18 transport and phosphorylation (expressed as the ‚lumped constant" ratio), Fludeoxyglucose F 18 is used to assess glucose metabolism. In comparison to background activity of the specific organ or tissue type, regions of decreased or absent uptake of Fludeoxyglucose F 18 reflect the decrease or absence of glucose metabolism. Regions of increased uptake of Fludeoxyglucose F 18 reflect greater than normal rates of glucose metabolism.

12.2 Pharmacodynamics

Fludeoxyglucose F 18 Injection is rapidly distributed to all organs of the body after intravenous administration. After background clearance of Fludeoxyglucose F 18 Injection, optimal PET imaging is generally achieved between 30 to 40 minutes after administration.

In cancer, the cells are generally characterized by enhanced glucose metabolism partially due to (1) an increase in activity of glucose transporters, (2) an increased rate of phosphorylation activity, (3) a reduction of phosphatase activity or, (4) a dynamic alteration in the balance among all these processes. However, glucose metabolism of cancer as reflected by Fludeoxyglucose F 18 accumulation shows considerable variability. Depending on tumor type, stage, and location, Fludeoxyglucose F 18 accumulation may be increased, normal, or decreased. Also, inflammatory cells can have the same variability of uptake of Fludeoxyglucose F 18.

In the heart, under normal aerobic conditions, the myocardium meets the bulk of its energy requirements by oxidizing free fatty acids. Most of the exogenous glucose taken up by the myocyte is converted into glycogen. However, under ischemic conditions, the oxidation of free fatty acids decreases, exogenous glucose becomes the preferred myocardial sub strate, glycolysis is stimulated, and glucose taken up by the myocyte is metabolized immediately instead of being converted into glycogen. Under these conditions, phosphorylated Fludeoxyglucose F 18 accumulates in the myocyte and can be detected with PET imaging.

In the brain, cells normally rely on aerobic metabolism. In epilepsy, the glucose metabolism varies. Generally, during a seizure, glucose metabolism increases. Interictally, the seizure focus tends to be hypometabolic.

12.3 Pharmacokinetics

Distribution: In four healthy male volunteers, receiving an intravenous administration of 30 seconds in duration, the arterial blood level profile for Fludeoxyglucose F 18 decayed triexponentially. The effective half-life ranges of the three phases were 0.2 to 0.3 minutes, 10 to 13 minutes with a mean and standard deviation (STD) of 11.6 (±) 1.1 min, and 80 to 95 minutes with a mean and STD of 88 (±) 4 min. Plasma protein binding of Fludeoxyglucose F 18 has not been studied.

Metabolism: Fludeoxyglucose F 18 is transported into cells and phosphorylated to [^{18}F]-FDG-6-phosphate at a rate proportional to the rate of glucose utilization within that tissue. [F18]-FDG-6-phosphate presumably is metabolized to 2-deoxy-2-[F18]fluoro-6-phospho-D-mannose([F 18]FDM-6-phosphate).

Fludeoxyglucose F 18 Injection may contain several impurities (e.g., 2-deoxy-2-chloro-D-glucose (ClDG)). Biodistribution and metabolism of ClDG are presumed to be similar to Fludeoxyglucose F 18 and would be expected to result in intracellular formation of 2-deoxy-2-chloro-6-phospho-D-glucose (ClDG-6-phosphate) and 2-deoxy-2-chloro-6-phospho-D-mannose (ClDM-6-phosphate). The phosphorylated deoxyglucose compounds are dephosphorylated and the resulting compounds (FDG, FDM, ClDG, and ClDM) presumably leave cells by passive diffusion. Fludeoxyglucose F 18 and related compounds are cleared from non-cardiac tissues within 3 to 24 hours after administration. Clearance from the cardiac tissue may require more than 96 hours. Fludeoxyglucose F 18 that is not involved in glucose metabolism in any tissue is then excreted in the urine.

Elimination: Fludeoxyglucose F 18 is cleared from most tissues within 24 hours and can be eliminated from the body unchanged in the urine. Three elimination phases have been identified in the reviewed literature. Within 33 minutes, a mean of 3.9% of the administrated radioactive dose was measured in the urine. The amount of radiation exposure of the urinary bladder at two hours post-administration suggests that 20.6% (mean) of the radioactive dose was present in the bladder.

Special Populations: The pharmacokinetics of Fludeoxyglucose F 18 Injection have not been studied in renally-impaired, hepatically impaired or pediatric patients. Fludeoxyglucose F 18 is eliminated through the renal system. Avoid excessive radiation exposure to this organ system and adjacent tissues. The effects of fasting, varying blood sugar levels, conditions of glucose intolerance, and diabetes mellitus on Fludeoxyglucose F 18 distribution in humans have not been ascertained [see Warnings and Precautions (5.2)].

13 NONCLINICAL TOXICOLOGY

13.1 Carcinogenesis, Mutagenesis, Impairment of Fertility

Animal studies have not been performed to evaluate the Fludeoxyglucose F 18 Injection carcinogenic potential, mutagenic potential or effects on fertility.

14 CLINICAL STUDIES

14.1 Oncology

The efficacy of Fludeoxyglucose F 18 Injection in positron emission tomography cancer imaging was demonstrated in 16 independent studies. These studies prospectively evaluated the use of Fludeoxyglucose F 18 in patients with suspected or known malignancies, including non-small cell lung cancer, colo-rectal, pancreatic, breast, thyroid, melanoma, Hodgkin's and non-Hodgkin's lymphoma, and various types of metastatic cancers to lung, liver, bone, and axillary nodes. All these studies had at least 50 patients and used pathology as a standard of truth. The Fludeoxyglucose F 18 Injection doses in the studies ranged from 200 MBq to 740 MBq with a median and mean dose of 370 MBq. In the studies, the diagnostic performance of Fludeoxyglucose F 18 Injection varied with the type of cancer, size of cancer, and other clinical conditions. False negative and false positive scans were observed. Negative Fludeoxyglucose F 18 Injection PET scans do not exclude the diagnosis of cancer. Positive Fludeoxyglucose F 18 Injection PET scans can not replace pathology to establish a diagnosis of cancer. Non-malignant conditions such as fungal infections, inflammatory processes and benign tumors have patterns of increased glucose metabolism that may give rise to false-positive scans. The efficacy of Fludeoxyglucose F 18 Injection PET imaging in cancer screening was not studied.

14.2 Cardiology

The efficacy of Fludeoxyglucose F 18 Injection for cardiac use was demonstrated in ten independent, prospective studies of patients with coronary artery disease and chronic left ventricular systolic dysfunction who were scheduled to undergo coronary revascularization. Before revascularization, patients underwent PET imaging with Fludeoxyglucose F 18 Injection (74 to 370 MBq, 2 to 10 mCi) and perfusion imaging with other diagnostic radiopharmaceuticals. Doses of Fludeoxyglucose F 18 Injection ranged from 74 to 370 MBq (2 to 10 mCi). Segmental, left ventricular, wall-motion assessments of asynergic areas made before revascularization were compared in a blinded manner to assessments made after successful revascularization to identify myocardial segments with functional recovery. Left ventricular myocardial segments were predicted to have reversible loss of systolic function if they showed Fludeoxyglucose F 18 accumulation and reduced perfusion (i.e., flow-metabolism mismatch). Conversely, myocardial segments were predicted to have irreversible loss of systolic function if they showed reductions in both Fludeoxyglucose F 18 accumulation and perfusion (i.e., matched defects). Findings of flow-metabolism mismatch in a myocardial segment may suggest that successful revascularization will restore myocardial function in that segment. However, false-positive tests occur regularly, and the decision to have a patient undergo revascularization should not be based on PET findings alone. Similarly, findings of a matched defect in a myocardial segment may suggest that myocardial function will not recover in that segment, even if it is successfully revascularized. However, false-negative tests occur regularly, and the decision to recommend against coronary revascularization, or to recommend a cardiac transplant, should not be based on PET findings alone. The reversibility of segmental dysfunction as predicted with Fludeoxyglucose F 18 PET imaging depends on successful coronary revascularization. Therefore, in patients with a low likelihood of successful revascularization, the diagnostic usefulness of PET imaging with Fludeoxyglucose F 18 Injection is more limited.

14.3 Neurology

In a prospective, open label trial, Fludeoxyglucose F 18 Injection was evaluated in 86 patients with epilepsy. Each patient received a dose of Fludeoxyglucose F 18 Injection in the range of 185 to 370 MBq (5 to 10 mCi). The mean age was 16.4 years (range: 4 months to 58 years; of these, 42 patients were less than 12 years and 16 patients were less than 2 years old). Patients had a known diagnosis of complex partial epilepsy and were under evaluation for surgical treatment of their seizure disorder. Seizure foci had been previously identified on ictal EEGs and sphenoidal EEGs. Fludeoxyglucose F 18 Injection PET imaging confirmed previous diagnostic findings in 16% (14/87) of the patients; in 34% (30/87) of the patients, Fludeoxyglucose F 18 Injection PET images provided new findings. In 32% (27/87), imaging with Fludeoxyglucose F 18 Injection was inconclusive. The impact of these imaging findings on clinical outcomes is not known. Several other studies comparing imaging with Fludeoxyglucose F 18 Injection results to subsphenoidal EEG, MRI and/or surgical findings supported the concept that the degree of hypometabolism corresponds to areas of confirmed epileptogenic foci. The safety and effectiveness of Fludeoxyglucose F 18 Injection to distinguish idiopathic epileptogenic foci from tumors or other brain lesions that may cause seizures have not been established.

15 REFERENCES

- 1. Gallagher B.M., Ansari A., Atkins H., Casella V., Christman D.R., Fowler J.S., Ido T., MacGregor R.R., Som P., Wan C.N., Wolf A.P., Kuhl D.E., and Reivich M. "Radiopharmaceuticals XXVII. ^{18}F-labeled 2-deoxy-2-fluoro-d-glucose as a radiopharmaceutical for measuring regional myocardial glucose metabolism in vivo: tissue distribution and imaging studies in animals," J Nucl Med, 1977; 18, 990-6.
- 2. Jones S.C., Alavi, A., Christman D., Montanez, I., Wolf, A.P., and Reivich M. "The radiation dosimetry of 2 [F-18] fluoro-2-deoxy-D-glucose in man," J Nucl Med, 1982; 23, 613-617.
- 3. Kocher, D.C. "Radioactive Decay Tables: A handbook of decay data for application to radiation dosimetry and radiological assessments," 1981, DOE/TIC-I 1026, 89.
- 4. ICRP Publication 53, Volume 18, No. I-4,1987, pages 75-76.

16 HOW SUPPLIED/STORAGE AND DRUG HANDLING

Fludeoxyglucose F 18 Injection is supplied in a multi-dose, capped 30 mL and 50 mL glass vial containing between 0.740 to 7.40 GBq/mL (20 to 200 mCi/mL), of no carrier added 2-deoxy-2-[F 18] fluoro-D-glucose, at end of synthesis, in approximately 15 to 50 mL.
The contents of each vial are sterile, pyrogen-free and preservative-free.
NDC 40028-511-30; 40028-511-50
Receipt, transfer, handling, possession, or use of this product is subject to the radioactive material regulations and licensing requirements of the U.S. Nuclear Regulatory Commission, Agreement States or Licensing States as appropriate.
Store the Fludeoxyglucose F 18 Injection vial upright in a lead shielded container at 25°C (77°F); excursions permitted to 15-30°C (59-86°F).
Store and dispose of Fludeoxyglucose F 18 Injection in accordance with the regulations and a general license, or its equivalent, of an Agreement State or a Licensing State.
The expiration date and time are provided on the container label. Use Fludeoxyglucose F 18 Injection within 12 hours from the EOS time.

17 PATIENT COUNSELING INFORMATION

Instruct patients in procedures that increase renal clearance of radioactivity.
Encourage patients to:
- drink water or other fluids (as tolerated) in the 4 hours before their PET study.
- void as soon as the imaging study is completed and as often as possible thereafter for at least one hour.

Manufactured by: PETNET Solutions Inc. 810 Innovation Drive Knoxville, TN 37932
Distributed by: PETNET Solutions Inc.^ 810 Innovation Drive Knoxville, TN 37932^
PETNET Solutions
PN0002262 Rev. A
Marcg 1, 2011

Indications

Fludeoxyglucose F18 Injection is indicated for positron emission tomography (PET) imaging in the following settings:

Oncology: For assessment of abnormal glucose metabolism to assist in the evaluation of malignancy in patients with known or suspected abnormalities found by other testing modalities, or in patients with an existing diagnosis of cancer.

Cardiology: For the identification of left ventricular myocardium with residual glucose metabolism and reversible loss of systolic function in patients with coronary artery disease and left ventricular dysfunction, when used together with myocardial perfusion imaging.

Neurology: For the identification of regions of abnormal glucose metabolism associated with foci of epileptic seizures.

Important Safety Information

Radiation Risks: Radiationemitting products, including Fludeoxyglucose F18 Injection, may increase the risk for cancer, especially in pediatric patients. Use the smallest dose necessary for imaging and ensure safe handling to protect the patient and healthcare worker.

Blood Glucose Abnormalities: In the oncology and neurology setting, suboptimal imaging may occur in patients with inadequately regulated blood glucose levels. In these patients, consider medical therapy and laboratory testing to assure at least two days of normoglycemia prior to Fludeoxyglucose F18 Injection administration.

Adverse Reactions: Hypersensitivity reactions with pruritus, edema and rash have been reported; have emergency resuscitation equipment and personnel immediately available.

Dosage Forms and Strengths: Multiple-dose 30 mL and 50 mL glass vial containing 0.74 to 7.40 GBq/mL (20 to 200 mCi/mL) of Fludeoxyglucose F^{18} injection and 4.5 mg of sodium chloride with 0.1 to 0.5% w/w ethanolas a stabilizer (approximately 15 to 50 mL volume) for intravenous administration. Fludeoxyglucose F^{18} injection is manufactured by Siemens' PETNET Solutions, 810 Innovation Drive, Knoxville, TN 39732, USA.

On account of certain regional limitations of sales rights and service availability, we cannot guarantee that all products included in this brochure are available through the Siemens sales organization worldwide. Availability and packaging may vary by country and is subject to change without prior notice. Some/All of the features and products described herein may not be available in the United States.

The information in this document contains general technical descriptions of specifications and options as well as standard and optional features which do not always have to be present in individual cases, and which may not be commercially available in all countries. Due to regulatory reasons their future availability cannot be guaranteed. Please contact your local Siemens organization for further details.

Siemens reserves the right to modify the design, packaging, specifications, and options described herein without prior notice. Please contact your local Siemens sales representative for the most current information.

Note: Any technical data contained in this document may vary within defined tolerances. Original images always lose a certain amount of detail when reproduced.

Profound Medical and Siemens have entered into a strategic agreement to further the development of prostate cancer care. The development of this whitepaper was supported by Siemens Healthcare GmbH and Profound Medical.

Siemens Healthineers Headquarters
Siemens Healthcare GmbH
Henkestr. 127
91052 Erlangen, Germany
Phone: +49 9131 84-0
siemens-healthineers.com

Published by Siemens Healthcare GmbH · Order No. A91MR-1100-98C-7600 · Printed in Germany ·